Geochimica et Cosmochimica Acta, Vol. 69, No. 21, pp. 5033–5060, 2005

0016-7037/05 $30.00 + .00

doi:10.1016/j.gca.2005.07.005

Multiple sulfur isotopes of sulfides from sediments in the aftermath of Paleoproterozoic glaciations

D. Papineau,[1,2,]* S. J. Mojzsis,[1,2] C. D. Coath,[3] J. A. Karhu,[4] and K. D. McKeegan[5]

[1]Department of Geological Sciences and
[2]Center for Astrobiology, University of Colorado, UCB399 Boulder, CO 80309-0399, USA
[3]Department of Earth Sciences, University of Bristol, Bristol, BS8 1RJ, United Kingdom
[4]Department of Geology, University of Helsinki, FIN-00014 Helsinki, Finland
[5]Department of Earth and Space Sciences, University of California, Los Angeles, CA 90095-1567, USA

(*Received March* 17, 2005; *accepted in revised form July* 5, 2005)

Abstract—Geochemical evidence reported from Paleoproterozoic sediments has long been used to evaluate the transition from the anoxic Archean atmosphere to an oxygenated atmosphere. Sulfur isotopes (^{32}S, ^{33}S, ^{34}S and ^{36}S) in sedimentary sulfides and sulfates are an especially sensitive means to monitor this transition, such that the timing of the Paleoproterozoic "Great Oxidation Event" can be investigated using mass-independently fractionated (MIF) sulfur isotope systematics expressed as Δ^{33}S. Here we report data from 83 individual analyses of pyrite, pyrrhotite and chalcopyrite on a new suite of 30 different samples from Finland, South Africa, Wyoming and Ontario that span ~600 My and follow one or several "Snowball Earth" events in the Paleoproterozoic. The samples were measured using a high-resolution secondary ion mass spectrometry technique in multicollection mode that investigates multiple sulfur isotopes in microdomains (<30 μm) within individual sulfide grains while preserving petrographic context. We focused on sediments deposited in the aftermath of the Paleoproterozoic glaciations (between 1.9 and 2.2 Ga) to trace fluctuations in atmospheric O_2 concentrations that were likely affected by an interplay of O_2 sinks in the atmosphere and the upper ocean and continental crust, and by the emergence and diversification of aerobic organisms. Our results demonstrate that MIF sulfur isotopes are absent in sediments deposited after the period of protracted global cooling in the Paleoproterozoic and independently confirm observations that MIF ceased during this time. We interpret our results by integrating Δ^{33}S and δ^{34}S data in sulfides, δ^{13}C data in carbonates and the estimated timing of glaciation events in the Paleoproterozoic. Data strongly hint at the presence of microbial sulfate reduction and fluctuations in the concentration of dissolved seawater sulfate and/or in $\delta^{34}S_{\text{sulfate}}$ in the aftermath of glaciations and likely were affected by changing erosion rates and nutrient delivery to the oceans. These changes modulated the population of primary producers, especially oxygenic photosynthesizers, and led to fluctuations in the abundance of atmospheric O_2, CO_2 and CH_4. Our results support the interpretation that the world-wide $\delta^{13}C_{\text{carb}}$ excursion observed between ~2.25 and 2.05 Ga (Karhu and Holland, 1996) was a period of significant accumulation of O_2 in the atmosphere. *Copyright © 2005 Elsevier Ltd*

1. INTRODUCTION

The evolution of microbial metabolisms was profoundly influenced by redox changes to the Paleoproterozoic (2.5–1.8 Ga) atmosphere and the rise in free molecular oxygen (Holland, 1984). Abundant O_2 on the contemporary Earth is produced from oxygenic photosynthesis, a light-driven metabolic pathway where H_2O is used as an electron donor to reduce CO_2, produce O_2 and sugars, and transfer electrons. The time of the emergence of this metabolic pathway is difficult to assess, but several lines of evidence such as organic biomarkers (e.g., 2α-methylhopanes) in 2.7 Ga shales from Western Australia have been used to propose the existence of oxygenic photosynthesis in the Archean (Brocks et al., 1999). Because they are sensitive to redox changes, the biogeochemical cycles of carbon (DesMarais et al., 1992), nitrogen (Beaumont and Robert, 1999; Papineau et al., 2005) and sulfur (Canfield and Raiswell, 1999; Farquhar et al., 2000) were fundamentally transformed during the transition from a global anoxic environment in the Archean, to the oxygenated atmosphere of the Proterozoic and Phanerozoic. Hence, the geochemistry of C-N-S in ancient sediments provides a valuable proxy for tracing the progressive oxidation of the surface environment.

Paleoproterozoic carbonates in marine sedimentary sequences worldwide are characterized by large carbon isotope excursions (Karhu, 1993; Karhu and Holland, 1996). Paleoproterozoic $\delta^{13}C_{\text{carb}}$ values[1] showing enrichment in ^{13}C are found in carbonate from North America (Melezhik et al., 1997; Bekker et al., 2003a), Baltica (Karhu and Melezhik, 1992; Karhu, 1993; Melezhik et al., 1999), Africa (Buick et al., 1998; Bekker et al., 2001), India (Sreenivas et al., 2001), South America (Bekker et al., 2003b) and Australia (Lindsay and Brasier, 2002). The $\delta^{13}C_{\text{carb}}$ maxima for these generally range between +7 to +13‰. One proposed interpretation used to explain these values is that there was a large increase in the rate of organic carbon burial from enhanced primary productivity for a large part of the Paleoproterozoic (Karhu and Holland, 1996) perhaps stimulated by increased tectonic activity around 2.1 Ga (e.g., Zhao et al., 2002). A more vigorous orogenic

---

* Author to whom correspondence should be addressed (dominic.papineau@colorado.edu).

[1] Where $\delta^{13}C_{\text{carb}}$ (‰) = $[(^{13}C/^{12}C)_{\text{carb}}/(^{13}C/^{12}C)_{\text{PDB}} - 1] \times 1000$.

Table 1. Description of analyzed samples.

Sample	Location		Age (Ga)	Petrology	Metamorphic grade	Mineralogy[a]	Sulfide phases
FIK97-7	N63°58′21.4″	E28°06′03.8″	~1.90–1.94	Two-mica schist	Amphibolite	Qtz + Bi − Ms − Su	Py
FIK97-11	N63°58′43.2″	E28°05′45.6″	~1.90–1.94	Mica schist	Amphibolite	Qtz + Bi + Su	Po
FIK66-1	N62°37′57.7″	E29°19′24.4″	~1.88–1.92	Mica schist	Amphibolite	Qtz + Bi + Su − Ap	Po
FIK118-2	N62°43′00.1″	E28°58′40.2″	~1.97	Quartz rock	Amphibolite	Qtz + Bi + Su − Tre − Act	Py
FIK119-8	N62°51′57.0″	E29°21′20.1″	~1.97	Black shale	Amphibolite	Ms + Gr + Su	Py
FIK97-1	N63°57′51.7″	E28°06′45.3″	~1.90–1.94	Mica schist	Amphibolite	Qtz + Ms + Su	Py + Po
FIK19-A	N62°31′33.4″	E29°51′41.0″	1.9–2.1	Black shale	Amphibolite	Qtz + Gr + Tre + Act + Su	Po
FIK64-2	N67°50′15.5″	E24°44′33.9″	~2.01	Black shale	Greenschist	Qtz + Bi + Su − Gr − Fe-Ti-Ox	Po
FI02006	N66°12′42.1″	E24°55′25.6″	2.06–2.09	Phyllitic quartzite	Greenschist	Qtz + Phl + Dol − Ti − Ox − Ap − Su	Py
FI02016	N66°12′42.1″	E24°55′25.6″	2.06–2.09	Phyllite	Greenschist	Qtz + Phl + Dol + Su	Py
FI02020	N66°12′43.1″	E24°56′24.0″	2.06–2.09	Dolomite	Lower greenschist	Dol − Phl − Su − Ti − Ox − Ap − REEP	Py + Ch
FI02021	N66°12′43.1″	E24°56′24.0″	2.06–2.09	Phyllite	Lower greenschist	Mi − Dol − Su	Ch
FI02024 (90.0m)	N65°57′34.6″	E24°28′46.6″	2.06–2.09	Dolomite	Lower greenschist	Dol + Qtz + Cal − Mi − Ap − REEP − Zr − Su	Py
FI02025 (75.5m)	N65°57′34.6″	E24°28′46.6″	2.06–2.09	Stromatolitic dolomite	Lower greenschist	Dol − Phl − Su	Py + Ch
FI02026 (69.1 m)	N65°57′34.6″	E24°28′46.6″	2.06–2.09	Stromatolitic dolomite	Lower greenschist	Dol − Phl − Su	Py
FI02027 (67.4 m)	N65°57′34.6″	E24°28′46.6″	2.06–2.09	Stromatolitic dolomite	Lower greenschist	Dol − Phl − Su − Ap	Py
FI02028 (66.7m)	N65°57′34.6″	E24°28′46.6″	2.06–2.09	Stromatolitic dolomite	Lower greenschist	Dol − Phl − Su	Py
FI02031 (54.8 m)	N65°57′34.6″	E24°28′46.6″	2.06–2.09	Quartzite	Lower greenschist	Qtz − Phl − Su	Py
FI02036 (30.0 m)	N65°57′34.6″	E24°28′46.6″	2.06–2.09	Dolomitic quartzite	Lower greenschist	Dol + Qtz − Su − Ap	Py
FI02038 (28.0 m)	N65°57′34.6″	E24°28′46.6″	2.06–2.09	Stromatolitic dolomite	Lower greenschist	Dol + Qtz − Su	Py
FI02040 (25.0 m)	N65°57′34.6″	E24°28′46.6″	2.06–2.09	Dolomitic quartzite	Lower greenschist	Dol + Qtz − Mi − Ap − Zr − Su	Py
FI02041 (20.0m)	N65°57′34.6″	E24°28′46.6″	2.06–2.09	Stromatolitic dolomite	Lower greenschist	Dol + Qtz − Mi − Su − Ap − Zr	Py
FI02043 (11.0m)	N65°57′34.6″	E24°28′46.6″	2.06–2.09	Stromatolitic dolomite	Lower greenschist	Dol + Qtz − Mi − Su	Py
FI02045 (0.0m)	N65°57′34.6″	E24°28′46.6″	2.06–2.09	Stromatolitic dolomite	Lower greenschist	Dol + Qtz − Mi − Su − Zr	Py + Ch
FI112-NMK-96	N65°57′45.3″	E24°38′37.4″	2.06–2.09	Quartzite	Greenschist	Qtz + Dol − Su	Py
FI02052	N66°03′23.2″	E25°25′44.9″	2.22–2.43	Quartzite schist	Greenschist	Qtz + Bi + Ho − Su − Ba	Ch
FI02055	N66°03′23.2″	E25°25′44.9″	2.22–2.43	Quartzite schist	Greenschist	Qtz + Bi − Ho − Mag − Su − Pr	Py
GF-7	—	—	1.878	Stromatolitic chert	Lower greenschist	Qtz − Dol − Su	Py
WY03010	N41°21′36.2″	WI06°15′58.5″	~2.05–2.25	Mudstone	Greenschist	Qtz + Dol − Ap − Zr − Su − Fe-Ox	Py
PPRGI414	—	—	2.516	Bedded black chert	Greenschist	Qtz − Su	Py

[a] Act = actinolite, Ap = apatite, Ba = barite, Bt = biotite, Cal = calcite, Ch = chalcopyrite, Dol = dolomite, Gr = graphite, Ho = hornblende, Mag = magnetite, Mi = mica, Ms = muscovite, Ox = oxide, Phl = phlogopite, Pr = prehnite, Py = pyrite, Po = pyrrhotite, Qtz = quartz, REEP = rare earth element-rich phosphate, Su = sulfides, Tre = tremolite, Zr = zircon.

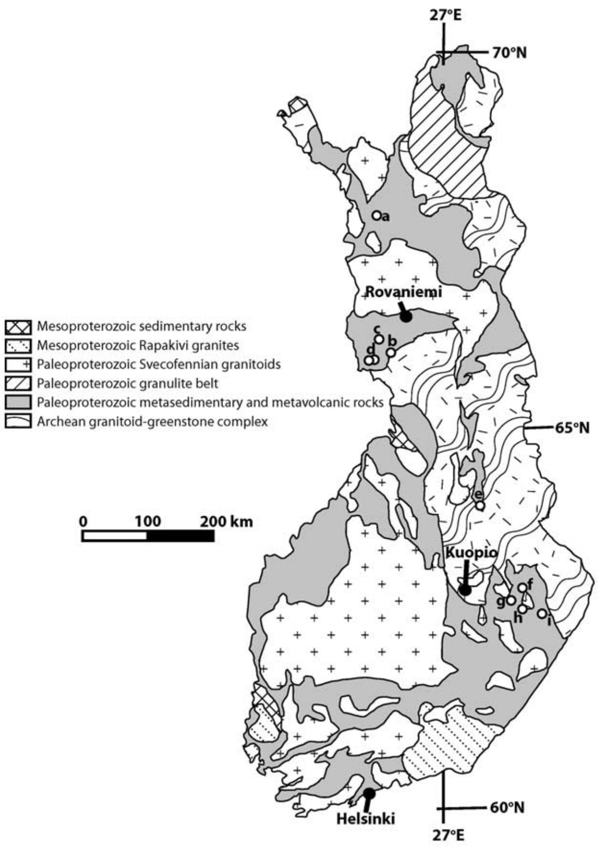

Fig. 1. Generalized geologic map of Finland with location of samples FIK64-2 (a); FI02052 and FI02055 (b); FI02006 to FI02021 (c); FI02024 to FI02045 and FI112-NMK-96 (d); FIK97-1, FIK97-7, and FIK97-11 (e); FIK119-8 (f); FIK118-2 (g); FIK66-1 (h); and FIK19-A (i). Map modified after "Bedrock map of Finland 1:10 000 000" (http://www.gsf.fi/welcome.html).

period along with a global expansion of the population of oxygenic photosynthetic bacteria could thereby have led to a rapid and perhaps irreversible increase in atmospheric O_2 once all major reducing reservoirs at the surface were exhausted. Punctuating the establishment of an oxygenated world that has typified Earth for the last 2 billion years were several episodes of widespread, possibly global glaciations in the Paleoproterozoic.

Key aspects of the Paleoproterozoic sulfur cycle were affected by the oxygenation of the atmosphere. Canfield and Raiswell (1999) compiled published sulfur isotopic data for sulfides from sediments of all ages and found that the range of $\delta^{34}S$ values[2] has generally increased with time. Canfield and coworkers have postulated that the evolution of $\delta^{34}S_{\text{sulfide}}$ values in Precambrian sediments reflects increases in the concentration of dissolved seawater sulfate due to the accumulation of substantial atmospheric O_2 (Canfield et al., 2000; Habicht et al., 2002). Recent data from mass-independently fractionated (MIF) sulfur isotopes (^{32}S, ^{33}S, ^{34}S, and ^{36}S)[3] buttress evidence in support of a major compositional change in the Paleoproterozoic atmosphere and transformation of the global sulfur cycle (Farquhar et al., 2000). Solar ultraviolet radiation penetrated deep into the Archean atmosphere due to the lack of an ozone screen (thereby indicating a virtual absence of atmospheric O_2) and imparted MIF to sulfur isotopes that was preserved in the sedimentary record (Farquhar et al., 2000). Archean sedimentary sulfides and sulfates often have MIF signatures with $|\Delta^{33}S| > 0.30‰$ (Farquhar et al., 2000; Hu et al., 2003; Mojzsis et al., 2003; Ono et al., 2003), which stands in contrast with almost all sulfides and sulfates younger than 2.0 Ga (Farquhar and Wing, 2003). Chemical speciation models suggest that MIF sulfur isotopic signals can be preserved only in an atmosphere containing $<10^{-5}$ PAL O_2 (present atmospheric level; Pavlov and Kasting, 2002). In principle, the timing of the transition from an anoxic atmosphere through to the axiomatic $\sim 10^{-5}$ PAL O_2 threshold can be constrained by following the demise of MIF sulfur isotopes in the geological record. Present data indicate that this transition occurred sometime between the last appearance of MIF sulfur in the 2.47 Ga Western Australian Brockman Iron Formation (Farquhar et al., 2000; Mojzsis et al., 2003) and the 2.32 Ga South African Timeball Hill Formation reported to have only mass-dependently fractionated (MDF) sulfur isotopes in sedimentary sulfide nodules (Bekker et al., 2004). However, the quantity of $\Delta^{33}S$ data and the provenance of the ancient sediments so far analyzed are insufficient to assess the rate and nature of the oxygenation of the atmosphere, a process that was very likely governed by a number of important O_2 sinks. Levels of atmospheric O_2 were likely affected by the interplay of reduced cation species in the upper ocean (e.g., Fe^{2+} and Mn^{2+}), weathering of crustal sulfides and organic matter, reduced atmospheric gases (e.g., CH_4), and the emergence, diversification and expansion of aerobic eukaryotes and microorganisms that perform aerobic heterotrophy, sulfide oxidation, methanotrophy and nitrification.

Here, we explore the record of multiple sulfur isotopes in sulfides from various Paleoproterozoic sediments collected in Finland, South Africa, Ontario (Canada) and Wyoming that have ages between 1.88 and 2.52 Ga. We specifically focus on a suite of sedimentary rocks dated between ~1.9 and 2.2 Ga to trace potential fluctuations in the atmospheric O_2 concentration in the aftermath of the three Paleoproterozoic glaciations (Bekker et al., 2005) and during a global carbonate carbon isotope excursion (Karhu and Holland, 1996). It is interesting to explore whether the downfall of MIF sulfur isotopes could have been temporarily reversed if the various O_2 sinks were rejuvenated. In principle, such reversals could have led to the effective collapse of an incipient transitory ozone screen from the de-oxygenation of the atmosphere that might be recorded in $\Delta^{33}S$ from Paleoproterozoic sediments before the system reached steady state. A high-resolution subset of sulfides from a sequence of stromatolitic dolomites of the 2.06–2.09 Ga

---

[2] Reported as $\delta^{3X}S_{CDT}$ (‰) = $[(^{3X}S/^{32}S)/(^{3X}S/^{32}S)_{CDT} - 1] \times 1000$, where X is either 3 or 4 and CDT is the sulfur isotope reference Cañon Diablo Troilite.

[3] Mass-independently fractionated sulfur isotopes are reported as permil deviations from the mass fractionation line defined by $\Delta^{33}S = 0‰$ (where $\Delta^{33}S$ (‰) = $1000 \times [(1 + \delta^{33}S/1000) - (1 + \delta^{34}S/1000)^{\lambda}]$; λ expresses the mass-dependent fractionation relationship between $\delta^{33}S$ and $\delta^{34}S$).

Table 2. Electron microprobe analyses of sulfide standard grains.

Standard grain[a]	Fe	S	Co	Ni	Cu	Zn	Total
1a	61.50	37.36	0.0271	0	0.0099	0	98.89
1b	60.42	36.48	0.0125	0.0209	0.0409	0.0078	96.98
1c	61.20	37.11	0.0425	0	0	0.0312	98.38
1e	62.38	36.69	0.0572	0	0	0.0500	99.18
2b	29.93	35.32	0.0058	0	33.66	0.0517	98.97
2c	29.78	35.29	0.0464	0.0117	34.75	0.0654	99.94
2e	29.83	34.92	0.0280	0	34.51	0.0759	99.37
3b	47.11	54.54	0.0456	0	0.0314	0.0032	101.73
3c	45.58	53.28	0.0435	0	0.0013	0.0206	98.93
3d	46.81	54.12	0.0297	0	0.0088	0.0222	100.99
3e	47.18	54.61	0.0350	0	0	0.0222	101.84
4a	44.08	50.54	0.0796	0.0100	0	0.0016	94.71
4b	46.92	54.31	0.0329	0	0	0.0190	101.29
4c	46.63	54.18	0.0350	0	0	0.0222	100.87
4d	46.94	54.52	0.0690	0	0.0351	0.0016	101.57
5a	59.60	40.10	0.1267	0	0	0	99.83
5b	59.46	39.69	0.0581	0.0077	0.0136	0.0203	99.24
5c	59.59	39.39	0.0695	0.0164	0	0	99.07
6a	59.01	39.95	0.0601	0.4018	0.0086	0	99.43
6c	59.23	39.96	0.0414	0.3871	0.0283	0	99.65
7c	29.60	35.29	0.0067	0	34.85	0.0135	99.77

[a] Standard grain labels comprise a number and a letter referring to the standard's name and to the grain number in the mount: 1 = CDT (tr), 2 = Trout Lake (ch), 3 = CAR 123 (py), 4 = Balmat (py), 5 = Anderson (po), 6 = LTB (po), and 7 = 7151 (ch).

Rantamaa Formation (Northern Finland) known to be associated with a large $\delta^{13}C_{carb}$ excursion (Karhu, 1993) was investigated to trace potential covariations between the sulfur and carbon cycles. All $\Delta^{33}S$ analyses were performed in situ on polished thin sections and grain-mounts using a secondary ion mass spectrometry (SIMS) technique that simultaneously measures the abundances of $^{32}S^-$, $^{33}S^-$ and $^{34}S^-$ ions at high mass resolution (Mojzsis et al., 2003). This technique preserves the petrographic context of sulfide grains in individual rock samples, which helps in the assessment of the origin of the sulfur being analyzed. We report 83 individual sulfur isotopic analyses of pyrite, pyrrhotite and chalcopyrite on 30 separate Paleoproterozoic sedimentary rocks; this work effectively expands the current inventory of published $\Delta^{33}S$ data by a factor of 2 for the Paleoproterozoic.

2. ANALYTICAL METHODS

2.1. Sample Preparation

An overview of each sample is presented in Table 1 and detailed descriptions of individual samples are given below. The provenance of our sample subset from Finland is shown on the generalized geologic map in Figure 1. Optically polished 2.54 cm round petrographic thin sections of hand samples were prepared using 0.05 μm alumina paste. Since the alumina paste is an aqueous suspension, care was taken to minimize surface oxidation of the sulfides in the polishing process. All thin sections and the sulfide grains hosted within them were mapped by reflected and transmitted light microscopy. The phase and trace metal chemistry of target sulfides were determined by wavelength dispersive spectroscopy (WDS) using the JEOL JXA-8600 electron microprobe (EMPA) at the Department of Geological Sciences, University of Colorado–Boulder. Trace metal analysis standards were the MAC pyrite (Fe and S) and pure metals for the other elements (Cu, Ni, Co, and Zn). Standard operating conditions were a 15 kV accelerating potential and electron beam current of ~21 nA. Following electron microprobe characterization, the thin sections were repolished with alumina paste, cleaned, dried with compressed nitrogen and then sputter-coated with ~100 Å layer of gold in preparation for ion microprobe analysis following our usual procedures (Greenwood et al., 2000).

Samples of carbonate were analyzed for their carbon and oxygen isotopic composition at the Department of Geology, University of Helsinki. Sample fragments were powdered and then reacted with anhydrous phosphoric acid at 90°C and analyzed in a Finnigan Delta Advantage mass spectrometer equipped with a Gas Bench II for continuous flow analysis of carbonates. The reproducibility was better than 0.1‰ for the $\delta^{13}C_{PDB}$ values, and better than 0.2‰ for $\delta^{18}O_{SMOW}$.

2.2. Description of Sulfide Standards

A new ion microprobe sulfur standards mount (GM4) was made from a preselected suite of "standard" sulfide grains of various phases with a mean diameter ~100 μm, and placed on double-sided sticky tape (Mojzsis et al., 2003, and references therein). The grains were cast in Beuhler epoxide and polished with 0.05 μm alumina. Compositions of the standard sulfide grains determined by EPMA are detailed in Table 2. The purpose of these analyses was to verify phase purity of individual grains and to quantitatively evaluate the compositional homogeneity of these natural "standards." Until purely homogeneous synthetic sulfur isotope standards can be established for the ion microprobe it is essential to precharacterize standards before analysis. Given that nearly all authigenic or paragenic sulfides present in sedimentary rocks are represented by pyrite, pyrrhotite and chalcopyrite, our standards mount does not explore the rich sulfide chemistry of Pb, As, Mo etc. Two pyrite standards were used for this study: CAR 123 which has $\delta^{34}S_{CDT}$ of $+1.41 \pm 0.2$‰ (Chaussidon, 1988) and Balmat which has a $\delta^{34}S_{CDT}$ of $+15.1 \pm 0.2$‰ (Crowe and Vaughan, 1996). The pyrrhotite standards we used included Anderson ($\delta^{34}S_{CDT} = +1.4 \pm 0.3$‰; Crowe and Vaughan, 1996) and LTB ($\delta^{34}S_{CDT} = -0.32 \pm 0.2$‰). Electron microprobe analysis of grains from LTB revealed a relatively high Ni content (~0.4%; Table 2) and associated pentlandite. Our two standards of chalcopyrite included Trout Lake ($\delta^{34}S_{CDT} = +0.3 \pm 0.3$‰; Crowe and Vaughan, 1996) and 7151 ($\delta^{34}S_{CDT} = +2.29 \pm 0.2$‰; Chaussidon, 1988).

2.3. High-Resolution Multicollector Ion Microprobe Technique

Instrumental methods are the same as described previously (Mojzsis et al., 2003) except as follows. A liquid nitrogen cold finger was used in the sample chamber to lower the partial pressure of water vapor and thus decrease potential contributions from scattered $^{32}SH^-$. The mean time per analysis was ~470 s, comprising ~200 s of presputtering; 15

Table 3. Instrumental mass fractionation for sulfide standards and phase.

Standard	Phase	$\delta^{34}S_{CDT}$ (‰)[a]	$^{34}S/^{32}S$[b]	$\delta^{34}S_{IMF}$ (‰)	±1σ (‰)	Weighted mean $\delta^{34}S_{IMF}$ (‰)[c]	±1σ (‰)	$\delta^{33}S_{IMF}$ (‰)[d]
January 2004 session								
CDT	Troilite	0.00	0.044163	−8.30	0.13	−8.30	0.13	−4.23
Trout Lake	Chalcopyrite	+0.30	0.044176	−2.61	0.07	−2.41	0.22	−1.23
7151	Chalcopyrite	+2.29	0.044264	−2.18	0.08			
CAR123	Pyrite	+1.41	0.044225	−2.98	0.12	−1.80	0.55	−0.92
Balmat	Pyrite	+15.10	0.044829	−1.55	0.05			
Anderson	Pyrrhotite	+1.40	0.044224	−6.06	0.05	−6.10	0.11	−3.11
LTB	Pyrrhotite	−0.32	0.044148	−6.38	0.12			
June 2004 session								
CDT	Troilite	0.00	0.044163	−2.31	0.28	−2.31	0.28	−1.17
CAR123	Pyrite	+1.41	0.044225	+3.07	0.15	+3.65	0.51	+1.85
Balmat	Pyrite	+15.10	0.044829	+4.11	0.13			
Anderson	Pyrrhotite	+1.40	0.044224	−0.44	0.12	−0.44	0.12	−0.22

[a] Independently measured sulfur isotopic compositions (see text). The $(^{34}S/^{32}S)_{CDT}$ is 0.0441626 (Ding et al., 2001).

[b] Measured ratio uncorrected for IMF.

[c] Weighted mean IMF for each sulfide phase.

[d] $\delta^{33}S_{IMF} = [(1 + \delta^{34}S_{IMF}/1000)^{\ln(m33/m32)/\ln(m34/m32)} - 1] \times 1000$, where m32, m33 and m34 are the masses of ^{32}S, ^{33}S and ^{34}S, respectively.

cycles of data acquisition at 10 s per cycle; and ~120 s setup time between analyses (to move from one analyte to another). Secondary-ion beam intensities were ~10^9, 10^7 and 5×10^7 ions per second for $^{32}S^-$, $^{33}S^-$ and $^{34}S^-$, respectively. There were two analytical sessions, one in January and another in June 2004, detailed as follows [June's session in brackets]: 137 [15] separate analyses on seven sulfide standards, 73 [10] analyses on 62 [6] sulfide grains from 27 [3] different samples. The measurements reported here have external errors (reproducibility of the standards excluding CDT) of: ±0.66 [0.63]‰, ±0.36 [0.29]‰, and ± 0.096 [0.095]‰ (2σ) for $\delta^{34}S$, $\delta^{33}S$, and $\Delta^{33}S$, respectively. The reproducibility of the Faraday detector baselines in ions per second (2σ) were 8000, 800, and 800 for the $^{32}S^-$, $^{33}S^-$, and $^{34}S^-$ detectors, respectively.

2.4. Data Reduction

We treated data for each analytical session independently. Steps taken in the data reduction can be summarized as follows: a) subtraction of detector baselines from the secondary-ion beam intensities; b) calculation of the $^{34}S/^{32}S$ instrumental mass-fractionation $IMF_{34/32}$ for each standard by taking the ratio of the mean, baseline-corrected instrumental $^{34}S/^{32}S$ value to the "true ratio" (independently measured); c) where analyses of more than one standard of a given sulfide phase exist, we took the weighted mean of the IMFs to be the $IMF_{34/32}$ for that phase; d) correcting all analyses for IMF by dividing the baseline-corrected ratio by the IMF for the corresponding phase. The instrumental mass-fractionation for the $^{33}S/^{32}S$ ratio ($IMF_{33/32}$) was calculated from $IMF_{34/32}$ by assuming an exponential law (Russell et al., 1978), i.e., $IMF_{33/32} = (IMF_{34/32})^{\ln(m33/m32)/\ln(m34/m32)}$, where m32, m33, and m34 are the masses of ^{32}S, ^{33}S, and ^{34}S respectively. Detector baselines measured at intervals throughout the sessions showed no drift with time, so averaged values were used for baseline-correction. Internal standard errors and correlations for each analysis were calculated from 15 pairs of ratios, one pair per measurement cycle. The errors and correlation are propagated to the internal standard error of the calculated $\Delta^{33}S$. It was found that the contribution from the correlation was small and could be neglected. The overall reported error is the combination of the internal and external error, which, in almost all analyses, is dominated by the latter. The IMFs for each standard and the weighted mean IMFs for each phase, expressed as permil deviations from unity, are shown in Table 3.

3. SAMPLES AND RESULTS

3.1. Mass-Dependent Fractionation

Mass-dependently fractionated sulfur isotopes behave predictably on a sulfur three-isotope plot (Hulston and Thode, 1965). The predictability of MDF laws for three isotopes arises from kinetic and equilibrium reactions that fractionate sulfur isotopes in approximate proportion to their relative mass difference. Mass-dependent fractionation processes for sulfur leads to a variation in isotopic compositions which can be described by the equation $(^{33}S/^{32}S) = k(^{34}S/^{32}S)^{\lambda}$, where k and λ are constants. This equation can be written

$$(^{33}S/^{32}S)/(^{33}S/^{32}S)_{CDT} = [(^{34}S/^{32}S)/(^{34}S/^{32}S)_{CDT}]^{\lambda}.$$

Therefore, linear regression in (x,y) with $y = \ln(^{33}S/^{32}S)$ and $x = \ln[(^{34}S/^{32}S)/(^{34}S/^{32}S)_{CDT}]$ has slope λ. York regression through data taken from our standards measurements, internal errors, yields: first session (n = 137), $\lambda = 0.5180 \pm 0.0013$,[4] MSWD[5] = 2.7; second session (n = 15) $\lambda = 0.5176 \pm 0.0036$, MSWD = 2.0 (errors are 2σ). These values are consistent with $\lambda = 0.518$ used by Farquhar et al. (2000) so we adopt this value for the computation of $\Delta^{33}S$. With the slope fixed at 0.518 and defining $(^{34}S/^{32}S)_{CDT} = (22.6436)^{-1}$ (Ding et al., 2001) regression through the standard data (York, fixed slope) was used to find the intercept, $\ln[(^{33}S/^{32}S)_{CDT}]$. The results for this analysis are: January 2004 session $(^{33}S/^{32}S)_{CDT} = 0.007908$; June 2004 session $(^{33}S/^{32}S)_{CDT} = 0.007881$. The discrepancy between the two sessions is accounted for by uncertainty in the calibration of the relative gain of the detector amplifiers. However, since $\delta^{33}S_{CDT}$ is calculated relative to this session-dependent reference ratio, there is no resulting session-dependent bias in the reported figures.

The standards show a narrow range in $\Delta^{33}S$ of ± 0.1‰ (2σ) about zero. This scatter slightly exceeds the internal analytical precision and thus may reflect additional sources of error, or the scatter may reflect real heterogeneity resulting from different modes of mass-dependent fractionation among the "standards" (Young et al., 2002). Because of this intrinsic ambiguity, we

---

[4] The error given here is the York standard error multiplied by $(MSWD)^{1/2}$ to account for scatter in the data in excess of that implied by the error assigned to each data point.

[5] The MSWD is the mean square of the weighted deviates, or reduced χ^2.

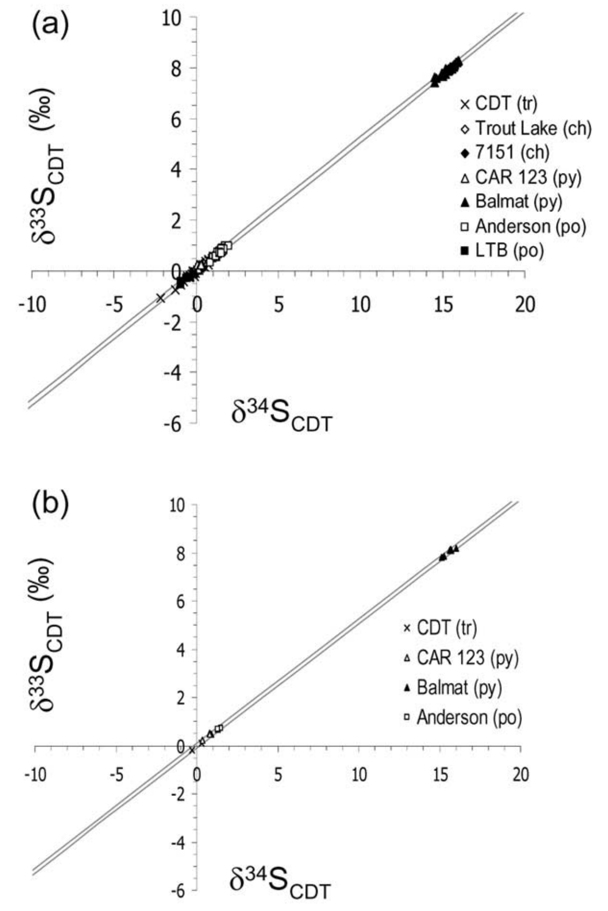

Fig. 2. Three-isotope plots for individual standard analyses for (a) January 2004 (n = 137) and (b) June 2004 (n = 15) sessions. More than 97% of standard analyses plotted within York-MDF band. Slopes calculated from standards are $\lambda = 0.5174 \pm 0.0015$ (2σ) for January session and $\lambda = 0.5179 \pm 0.004$ (2σ) for June session. A slope of 0.518 was used for calculation of $\Delta^{33}S$ (see text).

prefer to plot the MDF trajectory as a band rather than the more traditional line. The width of the band is defined by the standard deviation in y about the fixed-slope York regression through all the standard data in (x,y)-space using a slope of 0.518. When transformed to ($\delta^{34}S_{CDT}$, $\delta^{33}S_{CDT}$) space, the MDF band boundaries project as shallow curves so that the band width ($\sim\pm0.1$‰, 2σ) increases slightly with increasing $\delta^{34}S_{CDT}$ (Fig. 2). Deviations from MDF ($\Delta^{33}S$) are calculated using the formula $\Delta^{33}S$ (‰) $= 1000 \times [(1 + \delta^{33}S/1000) - (1 + \delta^{34}S/1000)^{0.518}]$; values which fall outside the band of MDF are considered to have resolvable $\Delta^{33}S$ anomalies.

Standard data (Table 4) are shown on a three isotope plot in Figure 2. From these data, we note a correlation between sulfide phase, ion count rate and IMF (Fig. 3). The range of average ^{32}S intensity for pyrite is similar to that of chalcopyrite and these phases generally contribute higher ion counts per second than pyrrhotite or troilite, which has the lowest ion yield (Fig. 3a). The correlation between $\delta^{34}S_{IMF}$ and ^{32}S intensity indicates higher IMF with decreasing ^{32}S count rates. The $\delta^{34}S_{IMF}$ for the various standards (Table 3) also exhibits a significant correlation with the Fe/S ratio of sulfides as shown in Figure 3b. An increase in the Fe/S ratio of a sulfide corresponds to higher IMF, which, if taken with the correlation of higher IMF with decreasing ^{32}S count rates, indicates that high Fe content in sulfides results in lower count rates.

3.2. Results for Paleoproterozoic Samples

The samples for this study were specifically chosen from a suite of Paleoproterozoic sediments with sulfide occurrences. Each sample sulfide was optically mapped in reflected and transmitted light and chemically analyzed by electron microprobe WDS to determine the phase to apply the appropriate IMF correction. Chemical analyses are presented in Table 5. It should be noted that multiple sulfide phases occur in individual samples, which illustrates the importance of precharacterization by electron microprobe. Results for the sulfur isotopic composition of sample sulfides corrected for IMF with respect to their phase are presented in Table 6 and discussed in detail below.

3.2.1. Kainuu Belt (samples FIK97-7, FIK97-11, and FIK97-1)

The samples were collected from the lower Kalevian Sotkamo Group (FIK97-1) and from the upper Kalevian Nuasjärvi Group (FIK97-7 and FIK97-11) of the Talvivaara area in Kainuu, Finland. The rocks are mica schists that represent turbiditic deep-water greywackes with intercalated black shales (Lukkarinen and Lundqvist, 2000). The local geology of the Talvivaara area has been described by Loukola-Ruskeeniemi and Heino (1996). A U-Pb study of detrital zircons from an upper Kalevian metagreywacke from the Jormua area in the Kainuu Belt yielded ages between 1.94 and 2.06 Ga, which was interpreted to provide a maximum depositional age for the upper Kalevian assemblage (Claesson et al., 1993). The turbidites and black shales of the Kainuu Belt were subsequently deformed and metamorphosed to low pressure amphibolite facies during the Svecofennian orogeny at 1.9–1.8 Ga. Sulfides in these samples include pyrite and pyrrhotite as relatively large subhedral to anhedral crystals in a matrix of quartz and mica. Pyrite grains in FIK97-7 and the pyrrhotite grains in FIK97-11 are surrounded by quartz and biotite (Fig. 4a and b). Ion microprobe analyses of these three grains revealed $\Delta^{33}S$ values between -0.05 and $+0.06$‰ and $\delta^{34}S$ values between -9.01 and -13.07‰ ($n = 3$). Similarly, the analyzed subhedral pyrite and pyrrhotite crystals in sample FIK97-1 have $\Delta^{33}S$ values of $+0.01$ and $+0.05$‰ and $\delta^{34}S$ values of -3.08 and -3.19‰ ($n = 2$; Fig. 4c).

3.2.2. Outokumpu schist (sample FIK66-1)

The sample was collected from the Upper Kalevian Outokumpu schist exposed at the Ratasuo locality, Liperi, Finland. The schists form allochthonous sequences emplaced onto the Archean craton margin (Koistinen, 1981). They are monotonous, thick-bedded metaturbidites with black shale interbeds (Lukkarinen and Lundqvist, 2000). The youngest $^{207}Pb/^{206}Pb$ age of 1920 Ma for detrital zircons of the Outokumpu turbidites represents the maximum depositional age for the succession (Claesson et al., 1993). The 1.88–1.92 Ga old Outokumpu schist contains abundant subhedral to anhedral pyrrhotite crys-

Table 4. Multicollector ion microprobe sulfur isotopic analyses of standard grains.

Grain spot[a]	$^{34}S/^{32}S$	$\pm 1\sigma$	$^{33}S/^{32}S$	$\pm 1\sigma$	^{32}S average intensity	$\delta^{34}S_{CDT}$ (‰)	$\pm 2\sigma$ (‰)	$\delta^{33}S_{CDT}$ (‰)	$\pm 2\sigma$ (‰)	$\Delta^{33}S$ (‰)	$\pm 2\sigma$ (‰)
January '04 session											
					Troilite (tr)						
CDT											
1a@1	4.415E-02	2.1E-06	7.906E-03	4.3E-07	9.46E+08	−0.35	0.68	−0.26	0.38	−0.08	0.15
1a@2	4.415E-02	1.2E-06	7.908E-03	3.7E-07	9.06E+08	−0.21	0.67	0.00	0.37	+0.11	0.15
1a@3	4.417E-02	1.1E-06	7.908E-03	3.0E-07	9.60E+08	+0.06	0.67	+0.01	0.37	−0.02	0.12
1a@4	4.416E-02	1.8E-06	7.907E-03	2.6E-07	9.18E+08	−0.11	0.68	−0.07	0.37	−0.01	0.12
1a@5	4.416E-02	1.6E-06	7.907E-03	3.4E-07	9.09E+08	−0.14	0.68	−0.10	0.37	−0.03	0.13
1a@6	4.416E-02	1.6E-06	7.906E-03	3.2E-07	9.32E+08	−0.09	0.68	−0.24	0.37	−0.19	0.11
1a@7	4.420E-02	1.9E-06	7.910E-03	4.2E-07	9.66E+08	+0.75	0.68	+0.21	0.38	−0.17	0.13
1a@8	4.419E-02	1.4E-06	7.911E-03	3.7E-07	9.45E+08	+0.57	0.68	+0.36	0.37	+0.06	0.13
1a@9	4.413E-02	1.7E-06	7.905E-03	3.0E-07	9.65E+08	−0.74	0.68	−0.41	0.37	−0.03	0.12
1a@10	4.418E-02	1.6E-06	7.909E-03	4.6E-07	9.63E+08	+0.34	0.68	+0.18	0.38	0.00	0.14
1b@1	4.423E-02	7.0E-07	7.914E-03	4.2E-07	8.95E+08	+1.46	0.67	+0.73	0.38	−0.03	0.14
1b@2	4.421E-02	8.3E-07	7.912E-03	3.3E-07	9.01E+08	+1.00	0.67	+0.54	0.37	+0.02	0.13
1b@3	4.420E-02	8.4E-07	7.911E-03	4.2E-07	8.66E+08	+0.74	0.67	+0.38	0.38	0.00	0.14
1b@4	4.417E-02	1.4E-06	7.909E-03	4.8E-07	8.51E+08	+0.19	0.67	+0.12	0.38	+0.03	0.14
1b@5	4.414E-02	1.2E-06	7.906E-03	5.3E-07	8.56E+08	−0.45	0.67	−0.25	0.39	−0.01	0.16
1b@6	4.415E-02	1.5E-06	7.907E-03	4.2E-07	8.75E+08	−0.26	0.68	−0.15	0.38	−0.02	0.15
1b@7	4.417E-02	1.1E-06	7.910E-03	3.9E-07	8.57E+08	+0.25	0.67	+0.22	0.37	+0.10	0.13
1b@8	4.417E-02	9.3E-07	7.908E-03	3.9E-07	9.50E+08	+0.19	0.67	+0.03	0.38	−0.07	0.14
1b@9	4.419E-02	8.6E-07	7.909E-03	4.1E-07	9.12E+08	+0.53	0.67	+0.16	0.38	−0.12	0.14
1c@1	4.420E-02	1.2E-06	7.911E-03	3.9E-07	9.06E+08	+0.76	0.67	+0.42	0.38	+0.03	0.14
1c@2	4.415E-02	1.4E-06	7.907E-03	2.9E-07	9.15E+08	−0.19	0.67	−0.07	0.37	+0.03	0.13
1c@3	4.416E-02	1.2E-06	7.907E-03	3.0E-07	9.24E+08	−0.07	0.67	−0.08	0.37	−0.05	0.12
1c@4	4.414E-02	1.2E-06	7.906E-03	3.5E-07	9.48E+08	−0.56	0.67	−0.22	0.37	+0.08	0.13
1c@5	4.407E-02	2.4E-06	7.899E-03	7.8E-07	4.94E+08	−2.17	0.68	−1.07	0.41	+0.05	0.22
1c@6	4.411E-02	1.3E-06	7.902E-03	4.2E-07	9.53E+08	−1.26	0.67	−0.74	0.38	−0.09	0.14
1c@7	4.417E-02	1.3E-06	7.909E-03	1.9E-07	9.31E+08	+0.24	0.67	+0.09	0.37	−0.03	0.12
1e@1	4.420E-02	7.4E-07	7.911E-03	3.5E-07	8.75E+08	+0.77	0.67	+0.44	0.37	+0.04	0.13
1e@2	4.418E-02	1.1E-06	7.910E-03	3.3E-07	8.40E+08	+0.42	0.67	+0.24	0.37	+0.02	0.13
1e@4	4.412E-02	9.1E-07	7.904E-03	3.9E-07	8.80E+08	−0.93	0.67	−0.55	0.38	−0.07	0.14
1e@5	4.415E-02	1.9E-06	7.906E-03	3.3E-07	9.12E+08	−0.35	0.68	−0.23	0.37	−0.05	0.12
1e@6	4.415E-02	9.5E-07	7.906E-03	3.5E-07	8.18E+08	−0.38	0.67	−0.19	0.37	0.00	0.13
					Chalcopyrite (ch)						
Trout Lake											
2b@1	4.417E-02	7.8E-07	7.909E-03	3.4E-07	1.36E+09	+0.20	0.67	+0.17	0.37	+0.06	0.13
2b@2	4.417E-02	8.1E-07	7.909E-03	2.8E-07	1.34E+09	+0.15	0.67	+0.11	0.37	+0.03	0.12
2c@1	4.418E-02	8.6E-07	7.910E-03	1.4E-07	1.35E+09	+0.37	0.67	+0.23	0.36	+0.04	0.10
2c@2	4.414E-02	4.4E-07	7.906E-03	2.0E-07	1.29E+09	−0.56	0.67	−0.26	0.37	+0.03	0.11
2c@3	4.417E-02	5.9E-07	7.908E-03	2.7E-07	1.33E+09	+0.19	0.67	+0.06	0.37	−0.03	0.12
2c@4	4.418E-02	7.8E-07	7.909E-03	3.9E-07	1.34E+09	+0.32	0.67	+0.18	0.38	+0.01	0.13
2c@5	4.417E-02	9.7E-07	7.909E-03	2.5E-07	1.40E+09	+0.19	0.67	+0.12	0.37	+0.02	0.11
2c@6	4.416E-02	4.4E-07	7.908E-03	3.3E-07	1.38E+09	−0.07	0.67	0.00	0.37	+0.03	0.13
2c@7	4.417E-02	7.2E-07	7.909E-03	2.7E-07	1.38E+09	+0.15	0.67	+0.12	0.37	+0.05	0.12
2c@8	4.417E-02	8.0E-07	7.909E-03	2.7E-07	1.38E+09	+0.21	0.67	+0.13	0.37	+0.02	0.12
2e@1	4.416E-02	5.9E-07	7.908E-03	2.9E-07	1.34E+09	−0.09	0.67	−0.02	0.37	+0.03	0.12
2e@2	4.417E-02	6.8E-07	7.909E-03	3.2E-07	1.33E+09	+0.12	0.67	+0.09	0.37	+0.02	0.12
7151											
7c@1	4.427E-02	7.7E-07	7.918E-03	2.2E-07	1.41E+09	+2.37	0.67	+1.24	0.37	+0.02	0.12
7c@2	4.427E-02	1.0E-06	7.918E-03	3.3E-07	1.41E+09	+2.41	0.67	+1.26	0.37	+0.01	0.12
7c@3	4.428E-02	9.0E-07	7.919E-03	3.4E-07	1.40E+09	+2.63	0.67	+1.38	0.37	+0.02	0.13
7c@4	4.428E-02	6.1E-07	7.919E-03	2.3E-07	1.41E+09	+2.67	0.67	+1.42	0.37	+0.04	0.11
					Pyrite (py)						
CAR 123											
3b@1	4.418E-02	6.3E-07	7.910E-03	3.6E-07	1.31E+09	+0.48	0.67	+0.30	0.37	+0.05	0.14
3b@2	4.418E-02	8.8E-07	7.910E-03	3.2E-07	1.31E+09	+0.35	0.67	+0.28	0.37	+0.09	0.13
3b@3	4.420E-02	9.3E-07	7.912E-03	4.1E-07	1.30E+09	+0.85	0.67	+0.58	0.38	+0.14	0.15
3b@4	4.415E-02	9.9E-07	7.907E-03	2.7E-07	1.34E+09	−0.26	0.67	−0.08	0.37	+0.06	0.12
3b@5	4.418E-02	1.0E-06	7.910E-03	2.9E-07	1.33E+09	+0.31	0.67	+0.24	0.37	+0.08	0.12
3c@1	4.419E-02	6.9E-07	7.911E-03	3.4E-07	1.30E+09	+0.68	0.67	+0.34	0.37	−0.01	0.13
3c@2	4.416E-02	8.9E-07	7.908E-03	2.4E-07	1.22E+09	−0.14	0.67	0.00	0.37	+0.07	0.12
3c@3	4.417E-02	9.3E-07	7.909E-03	3.0E-07	1.29E+09	+0.11	0.67	+0.08	0.37	+0.02	0.12
3c@4	4.419E-02	8.0E-07	7.911E-03	3.1E-07	1.27E+09	+0.68	0.67	+0.36	0.37	+0.01	0.12
3c@5	4.418E-02	1.1E-06	7.910E-03	2.1E-07	1.33E+09	+0.42	0.67	+0.27	0.37	+0.06	0.11
3c@6	4.420E-02	8.2E-07	7.911E-03	2.7E-07	1.30E+09	+0.81	0.67	+0.40	0.37	−0.01	0.12
3d@1	4.416E-02	9.5E-07	7.907E-03	3.7E-07	1.29E+09	−0.12	0.67	−0.05	0.37	+0.01	0.13

Table 4. (Continued)

Grain spot[a]	$^{34}S/^{32}S$	$\pm 1\sigma$	$^{33}S/^{32}S$	$\pm 1\sigma$	^{32}S average intensity	$\delta^{34}S_{CDT}$ (‰)	$\pm 2\sigma$ (‰)	$\delta^{33}S_{CDT}$ (‰)	$\pm 2\sigma$ (‰)	$\Delta^{33}S$ (‰)	$\pm 2\sigma$ (‰)
3d@2	4.417E-02	5.4E-07	7.910E-03	4.0E-07	7.38E+08	+0.08	0.67	+0.23	0.38	+0.19	0.14
3e@1	4.416E-02	5.4E-07	7.908E-03	2.9E-07	1.30E+09	+0.01	0.67	+0.04	0.37	+0.03	0.12
3e@2	4.418E-02	6.6E-07	7.909E-03	2.1E-07	1.26E+09	+0.33	0.67	+0.18	0.37	+0.01	0.11
3e@3	4.412E-02	1.8E-06	7.904E-03	3.1E-07	1.04E+09	−1.00	0.68	−0.52	0.37	0.00	0.12
Balmat											
4a@1	4.485E-02	5.1E-07	7.971E-03	2.6E-07	1.35E+09	+15.47	0.67	+7.95	0.37	−0.03	0.12
4a@2	4.486E-02	5.0E-07	7.972E-03	2.4E-07	1.34E+09	+15.70	0.67	+8.08	0.37	−0.02	0.11
4a@3	4.484E-02	5.5E-07	7.970E-03	2.6E-07	1.35E+09	+15.32	0.67	+7.89	0.37	−0.02	0.12
4a@4	4.483E-02	4.6E-07	7.969E-03	2.0E-07	1.36E+09	+15.12	0.67	+7.75	0.37	−0.06	0.11
4a@5	4.486E-02	6.3E-07	7.973E-03	2.0E-07	1.33E+09	+15.79	0.67	+8.19	0.37	+0.04	0.11
4a@6	4.483E-02	6.9E-07	7.970E-03	2.2E-07	1.29E+09	+15.18	0.67	+7.85	0.37	+0.02	0.11
4a@7	4.483E-02	7.6E-07	7.969E-03	2.9E-07	1.36E+09	+15.05	0.67	+7.77	0.37	+0.01	0.12
4a@8	4.484E-02	8.2E-07	7.970E-03	2.1E-07	1.37E+09	+15.25	0.67	+7.91	0.37	+0.04	0.11
4a@9	4.481E-02	7.9E-07	7.968E-03	1.9E-07	1.43E+09	+14.63	0.67	+7.59	0.37	+0.04	0.11
4a@10	4.480E-02	5.7E-07	7.968E-03	1.2E-07	1.46E+09	+14.54	0.67	+7.61	0.36	+0.11	0.10
4b@1	4.483E-02	7.6E-07	7.970E-03	3.3E-07	1.36E+09	+15.14	0.67	+7.79	0.37	−0.02	0.12
4b@2	4.485E-02	1.5E-06	7.971E-03	3.5E-07	1.34E+09	+15.58	0.68	+8.02	0.37	−0.02	0.12
4b@3	4.484E-02	5.2E-07	7.970E-03	2.9E-07	1.35E+09	+15.33	0.67	+7.88	0.37	−0.03	0.12
4b@4	4.484E-02	9.3E-07	7.970E-03	2.3E-07	1.34E+09	+15.26	0.67	+7.89	0.37	+0.02	0.11
4b@5	4.485E-02	4.0E-07	7.971E-03	2.2E-07	1.31E+09	+15.57	0.67	+7.98	0.37	−0.05	0.11
4b@6	4.482E-02	6.5E-07	7.969E-03	2.1E-07	1.36E+09	+14.97	0.67	+7.78	0.37	+0.05	0.11
4b@7	4.483E-02	8.7E-07	7.969E-03	2.5E-07	1.37E+09	+15.04	0.67	+7.75	0.37	−0.02	0.12
4c@1	4.484E-02	1.2E-06	7.970E-03	3.1E-07	1.33E+09	+15.25	0.67	+7.87	0.37	0.00	0.12
4c@2	4.484E-02	6.8E-07	7.970E-03	3.0E-07	1.34E+09	+15.23	0.67	+7.85	0.37	−0.01	0.13
4c@3	4.486E-02	4.1E-07	7.971E-03	2.5E-07	1.33E+09	+15.70	0.67	+8.02	0.37	−0.08	0.12
4c@4	4.485E-02	7.0E-07	7.971E-03	2.3E-07	1.33E+09	+15.47	0.67	+7.94	0.37	−0.04	0.12
4c@5	4.485E-02	9.0E-07	7.971E-03	3.0E-07	1.32E+09	+15.55	0.67	+7.98	0.37	−0.05	0.12
4c@6	4.484E-02	9.5E-07	7.971E-03	2.4E-07	1.32E+09	+15.44	0.67	+7.92	0.37	−0.05	0.12
4c@7	4.483E-02	6.3E-07	7.968E-03	3.3E-07	1.33E+09	+15.01	0.67	+7.64	0.37	−0.10	0.13
4c@8	4.483E-02	3.0E-07	7.971E-03	2.6E-07	1.46E+09	+15.21	0.67	+7.94	0.37	+0.09	0.12
4c@9	4.485E-02	8.4E-07	7.971E-03	3.3E-07	1.43E+09	+15.49	0.67	+8.01	0.37	+0.01	0.12
4c@10	4.486E-02	8.5E-07	7.973E-03	2.9E-07	1.41E+09	+15.86	0.67	+8.21	0.37	+0.03	0.12
4d@1	4.484E-02	7.1E-07	7.971E-03	2.1E-07	1.34E+09	+15.38	0.67	+7.95	0.37	+0.01	0.11
4d@2	4.485E-02	7.3E-07	7.972E-03	2.8E-07	1.33E+09	+15.63	0.67	+8.05	0.37	−0.02	0.12
4d@3	4.486E-02	7.4E-07	7.972E-03	2.4E-07	1.32E+09	+15.73	0.67	+8.10	0.37	−0.02	0.12
4d@4	4.486E-02	7.6E-07	7.973E-03	3.0E-07	1.32E+09	+15.89	0.67	+8.23	0.37	+0.03	0.12
4d@5	4.480E-02	4.9E-07	7.967E-03	2.8E-07	1.31E+09	+14.54	0.67	+7.42	0.37	−0.09	0.12
4d@6	4.483E-02	1.0E-06	7.969E-03	2.4E-07	1.32E+09	+15.19	0.67	+7.76	0.37	−0.08	0.11
4d@7	4.485E-02	8.5E-07	7.971E-03	2.7E-07	1.32E+09	+15.56	0.67	+7.98	0.37	−0.05	0.12
4d@8	4.483E-02	7.9E-07	7.969E-03	3.6E-07	1.32E+09	+15.14	0.67	+7.77	0.37	−0.04	0.13
4d@9	4.485E-02	6.8E-07	7.971E-03	2.8E-07	1.31E+09	+15.58	0.67	+7.96	0.37	−0.08	0.12
4d@10	4.485E-02	7.3E-07	7.971E-03	2.4E-07	1.30E+09	+15.47	0.67	+8.01	0.37	+0.03	0.11
4d@11	4.487E-02	9.3E-07	7.973E-03	2.1E-07	1.34E+09	+15.96	0.67	+8.27	0.37	+0.04	0.11
4d@12	4.486E-02	9.4E-07	7.972E-03	2.6E-07	1.32E+09	+15.71	0.67	+8.09	0.37	−0.01	0.11
					Pyrrhotite (po)						
Anderson											
5a@1	4.424E-02	5.8E-07	7.914E-03	3.5E-07	1.02E+09	+1.64	0.67	+0.79	0.37	−0.06	0.13
5a@2	4.423E-02	8.2E-07	7.915E-03	3.0E-07	1.01E+09	+1.61	0.67	+0.88	0.37	+0.04	0.13
5a@3	4.424E-02	7.0E-07	7.914E-03	3.0E-07	1.01E+09	+1.65	0.67	+0.79	0.37	−0.06	0.13
5a@4	4.424E-02	6.7E-07	7.915E-03	3.1E-07	1.00E+09	+1.74	0.67	+0.96	0.37	+0.06	0.13
5a@5	4.423E-02	9.1E-07	7.915E-03	3.5E-07	9.88E+08	+1.58	0.67	+0.88	0.37	+0.06	0.13
5a@6	4.422E-02	1.1E-06	7.913E-03	3.2E-07	9.70E+08	+1.26	0.67	+0.60	0.37	−0.05	0.12
5a@7	4.422E-02	5.2E-07	7.913E-03	2.9E-07	9.66E+08	+1.33	0.67	+0.70	0.37	+0.01	0.12
5a@8	4.422E-02	7.3E-07	7.914E-03	3.6E-07	9.68E+08	+1.41	0.67	+0.76	0.37	+0.03	0.13
5a@9	4.421E-02	4.6E-07	7.912E-03	3.3E-07	1.02E+09	+0.98	0.67	+0.47	0.37	−0.04	0.13
5a@10	4.421E-02	9.5E-07	7.912E-03	3.5E-07	1.01E+09	+1.01	0.67	+0.53	0.37	0.00	0.13
5a@11	4.420E-02	8.0E-07	7.910E-03	2.9E-07	9.98E+08	+0.88	0.67	+0.32	0.37	−0.13	0.12
5a@12	4.422E-02	6.7E-07	7.912E-03	3.6E-07	9.95E+08	+1.21	0.67	+0.54	0.37	−0.09	0.13
5a@13	4.423E-02	7.1E-07	7.915E-03	3.8E-07	9.91E+08	+1.58	0.67	+0.85	0.37	+0.03	0.14
5a@14	4.424E-02	5.7E-07	7.914E-03	3.4E-07	9.99E+08	+1.68	0.67	+0.83	0.37	−0.04	0.13
5a@15	4.423E-02	7.1E-07	7.915E-03	4.1E-07	9.94E+08	+1.55	0.67	+0.86	0.38	+0.06	0.14
5a@16	4.422E-02	7.3E-07	7.913E-03	3.4E-07	1.00E+09	+1.40	0.67	+0.71	0.37	−0.02	0.13
5a@17	4.423E-02	7.6E-07	7.913E-03	4.1E-07	1.00E+09	+1.51	0.67	+0.67	0.38	−0.11	0.14
5b@1	4.422E-02	7.5E-07	7.912E-03	2.6E-07	1.03E+09	+1.25	0.67	+0.51	0.37	−0.14	0.12
5b@2	4.422E-02	6.7E-07	7.913E-03	2.9E-07	1.03E+09	+1.35	0.67	+0.69	0.37	−0.01	0.12
5b@3	4.422E-02	6.0E-07	7.913E-03	3.2E-07	1.02E+09	+1.37	0.67	+0.68	0.37	−0.03	0.13
5b@4	4.423E-02	7.6E-07	7.914E-03	3.5E-07	1.01E+09	+1.58	0.67	+0.72	0.37	−0.09	0.14

Table 4. (Continued)

Grain spot[a]	$^{34}S/^{32}S$	$\pm 1\sigma$	$^{33}S/^{32}S$	$\pm 1\sigma$	^{32}S average intensity	$\delta^{34}S_{CDT}$ (‰)	$\pm 2\sigma$ (‰)	$\delta^{33}S_{CDT}$ (‰)	$\pm 2\sigma$ (‰)	$\Delta^{33}S$ (‰)	$\pm 2\sigma$ (‰)
5b@5	4.424E-02	7.7E-07	7.914E-03	3.0E-07	9.95E+08	+1.69	0.67	+0.81	0.37	−0.06	0.12
5b@6	4.425E-02	5.6E-07	7.916E-03	3.6E-07	1.04E+09	+2.00	0.67	+0.97	0.37	−0.07	0.14
5b@7	4.422E-02	4.8E-07	7.913E-03	3.2E-07	1.02E+09	+1.41	0.67	+0.70	0.37	−0.03	0.13
5b@8	4.423E-02	6.9E-07	7.914E-03	2.6E-07	1.02E+09	+1.53	0.67	+0.80	0.37	+0.01	0.12
5c@1	4.422E-02	5.1E-07	7.913E-03	4.9E-07	1.02E+09	+1.37	0.67	+0.66	0.38	−0.05	0.16
5c@2	4.423E-02	7.5E-07	7.914E-03	2.2E-07	1.02E+09	+1.63	0.67	+0.81	0.37	−0.03	0.11
5c@3	4.424E-02	8.7E-07	7.914E-03	4.9E-07	1.03E+09	+1.66	0.67	+0.78	0.38	−0.08	0.16
5c@4	4.421E-02	6.8E-07	7.912E-03	3.9E-07	9.96E+08	+1.01	0.67	+0.49	0.38	−0.03	0.14
LTB											
6a@1	4.412E-02	6.9E-07	7.904E-03	3.3E-07	9.86E+08	−0.93	0.67	−0.50	0.37	−0.02	0.13
6a@2	4.415E-02	8.6E-07	7.907E-03	2.4E-07	9.76E+08	−0.17	0.67	−0.12	0.37	−0.03	0.11
6a@3	4.414E-02	7.4E-07	7.906E-03	3.4E-07	9.75E+08	−0.53	0.67	−0.30	0.37	−0.02	0.13
6a@4	4.412E-02	6.9E-07	7.904E-03	2.9E-07	9.79E+08	−0.94	0.67	−0.43	0.37	+0.06	0.12
6c@1	4.414E-02	4.4E-07	7.905E-03	3.0E-07	9.85E+08	−0.59	0.67	−0.31	0.37	−0.01	0.12
6c@2	4.414E-02	9.7E-07	7.906E-03	3.5E-07	9.46E+08	−0.44	0.67	−0.27	0.37	−0.04	0.13
June 2004 session											
					Troilite (tr)						
CDT											
1a@1	4.418E-02	1.1E-06	7.882E-03	4.1E-07	5.38E+08	+0.28	0.64	+0.09	0.31	−0.06	0.14
1d@1	4.415E-02	1.7E-06	7.880E-03	3.5E-07	5.29E+08	−0.28	0.64	−0.21	0.31	−0.07	0.13
					Pyrite (py)						
CAR 123											
3a@1	4.420E-02	9.9E-07	7.885E-03	3.6E-07	7.78E+08	+0.90	0.64	+0.45	0.31	−0.02	0.13
3a@2	4.422E-02	7.5E-07	7.887E-03	2.4E-07	7.89E+08	+1.30	0.64	+0.67	0.30	−0.01	0.11
3d@1	4.418E-02	7.2E-07	7.883E-03	3.2E-07	7.59E+08	+0.37	0.64	+0.22	0.30	+0.03	0.13
3d@2	4.420E-02	9.3E-07	7.885E-03	2.5E-07	7.14E+08	+0.79	0.64	+0.50	0.30	+0.09	0.11
3d@3	4.420E-02	7.0E-07	7.885E-03	3.5E-07	7.39E+08	+0.81	0.64	+0.47	0.31	+0.05	0.13
Balmat											
1a@1	4.487E-02	6.3E-07	7.946E-03	2.9E-07	8.19E+08	+16.02	0.63	+8.18	0.30	−0.09	0.12
4b@1	4.486E-02	6.4E-07	7.945E-03	2.3E-07	7.77E+08	+15.70	0.63	+8.08	0.30	−0.02	0.11
4e@1	4.485E-02	5.8E-07	7.945E-03	2.4E-07	7.86E+08	+15.62	0.63	+8.08	0.30	+0.02	0.11
4e@2	4.486E-02	7.8E-07	7.946E-03	2.9E-07	7.83E+08	+15.68	0.64	+8.14	0.30	+0.05	0.12
4^{e}@3	4.483E-02	1.5E-06	7.943E-03	2.2E-07	7.32E+08	+15.10	0.64	+7.82	0.30	+0.02	0.11
4^{e}@4	4.484E-02	7.4E-07	7.943E-03	2.7E-07	7.42E+08	+15.27	0.64	+7.85	0.30	−0.03	0.12
					Pyrrhotite (po)						
Anderson											
5a@1	4.423E-02	7.6E-07	7.887E-03	3.7E-07	5.73E+08	+1.52	0.64	+0.71	0.31	−0.08	0.13
5a@2	4.422E-02	6.3E-07	7.887E-03	4.1E-07	5.74E+08	+1.28	0.63	+0.66	0.31	0.00	0.14

[a] Grain spot name starts with a number and a letter (see Table 2), followed by @number which designates the spot number on that grain.

tals randomly distributed in a quartz-biotite matrix (Fig. 5a). Ion microprobe analyses revealed that the sulfur isotopic composition of three pyrrhotite grains in sample FIK66-1 is between +5.31 and +5.94‰ for $\delta^{34}S$ and between +0.00 and +0.12‰ for $\Delta^{33}S$ ($n = 4$).

3.2.3. *Outokumpu association (samples FIK118-2 and FIK119-8)*

Samples were collected from drill core sections OKU95A/265.14 at the site of the former Keretti mine at Outokumpu and OKU857/221.80 in the Kylylahti area, Polvijärvi, Finland. The Outokumpu association consists of a serpentinite-black shale-carbonate rock-quartz rock assemblage, which is associated with the Outokumpu Cu-Co-Zn ore deposit (Koistinen, 1981). FIK118-2 was collected from the quartz rock unit and sample FIK119-8 is black shale. The Outokumpu association is now interpreted to be a remnant of ancient ophiolites (Lukkarinen and Lundqvist, 2000). The age of the complex is defined by a U-Pb zircon age of 1972 ± 18 Ma from a gabbroic body associated with serpentinite (Huhma, 1986). Geochemical and mineralogical arguments indicate that the origin of the Outokumpu quartz rock is not as detrital sediment. Recent studies have suggested derivation from a pervasively silicified ultramafic precursor, but a volcanic-exhalative origin and chemical precipitation on the sea floor have also been suggested (Lukkarinen and Lundqvist, 2000).

Sample FIK118-2 contains abundant subhedral to anhedral pyrite crystals with sizes from several to hundreds of microns randomly distributed in the quartz-dominated matrix. Duplicate analysis on a single grain (Fig. 5b) revealed negative $\delta^{34}S$ values of −23.46 and −23.68‰ and $\Delta^{33}S$ values of +0.30 and +0.24‰. Significantly, these values are even lower than the $\delta^{34}S$ range from −14.3 to −17.9‰ reported for the Outokumpu quartz rock by Mäkelä (1974). The metamorphosed Outokumpu black shale (FIK119-8) has been described by Loukola-Ruskeeniemi (1991). Data show that the black shale unit is characterized by an exceptionally high content of C_{org} and S, with average values around 7.0 and 7.2%wt, respectively. Reported $\delta^{13}C$ values for organic carbon that range between −19.1 and −29.7‰ and $\delta^{34}S$ values for pyrite, chal-

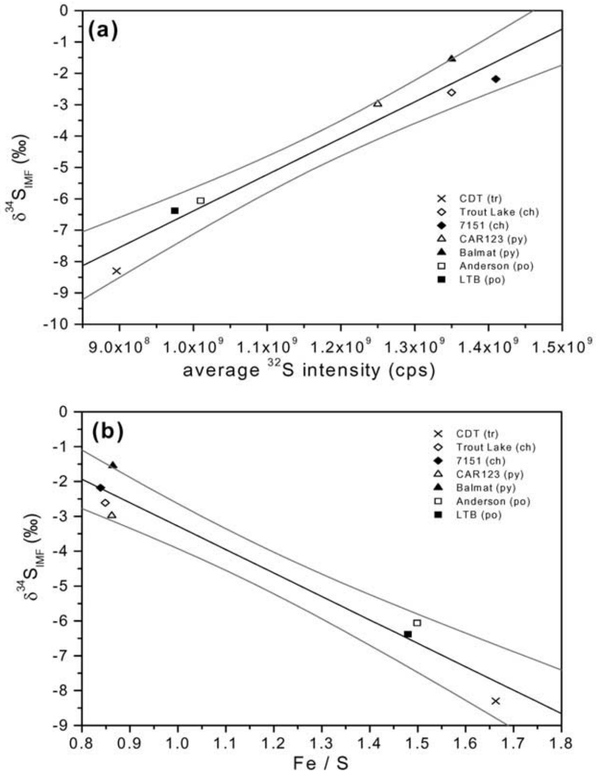

Fig. 3. (a) Correlation between $\delta^{34}S_{IMF}$ and ^{32}S counts per second (cps) for all analyses of each standard during January 2004 session. Linear fit through data (black line) is shown with 95.4% confidence interval bands (gray lines). (b) Linear fit of $\delta^{34}S_{IMF}$ and average Fe/S ratio (calculated from data in Table 2) for each sulfide standard analyzed during January 2004 session with 95.4% confidence intervals (gray lines).

copyrite and pyrrhotite varied between −2.3 and +4.2‰ (Loukola-Ruskeeniemi, 1991). The habit of pyrite grains of our wrinkly banded black shale sample FIK119-8 are often as large (hundreds of microns) euhedral crystals associated with muscovite bands (Fig. 5c). Two large grains were analyzed and found to have negative $\delta^{34}S$ values of −8.27 and −9.75‰ and $\Delta^{33}S$ values of +0.04 and +0.08‰.

3.2.4. *Mulo area (sample FIK19-A)*

This rock was collected from the Lower Kalevian Höytiäinen schists, east of the allochthonous Outokumpu schists, at the Mulo locality, Kiihtelysvaara, Finland. The Mulo area sample represents a calcareous black shale unit with abundant metamorphic actinolite bundles. Höytiäinen schists are composed of graded-bedded pelites and greywackes, with local coarse-clastic sediments deposited on a shelf or in a rifted basin environment (Lukkarinen and Lundqvist, 2000). The 1.9–2.1 Ga metamorphosed black shale sample FIK19-A contains abundant subhedral to anhedral crystals of pyrrhotite randomly distributed in the banded matrix of quartz and hornblende. Duplicate analyses on one grain and a single analysis on another revealed negative $\delta^{34}S$ values between −7.20 and −8.00‰ and $\Delta^{33}S$ values between −0.05 and +0.09‰ (Fig. 6a).

3.2.5. *Kittilä Group (sample FIK64-2)*

At the Veikasenmaa area of Finland, the Kittilä Group comprises mafic metavolcanic rocks, pyroclastic deposits and volcanic breccias as well as diabases and felsic porphyries (Rastas et al., 2001). About 200 m from the sample site, a felsic rhyolitic porphyry has been dated by U-Pb zircon to 2014 ± 8 Ma (Rastas et al., 2001). On the basis of field observations and geochemical data, the authors interpreted the felsic porphyry to be coeval with other supracrustal and subvolcanic rocks. Our ~2.01 Ga FIK64-2 sample is from a carbonaceous schist (black shale) unit of the Kittilä Greenstone Belt and contains large amounts of pyrrhotite blebs parallel to schistosity. Two pairs of large and elongated anhedral pyrrhotite crystals surrounded by microcrystalline quartz and biotite were selected for isotopic analysis by ion microprobe (Fig. 6b). Analyses on both pairs of grains from FIK64-2 revealed a small range of $\delta^{34}S$ values around −8‰ and $\Delta^{33}S$ values between +0.04 and +0.19‰ (n = 4).

3.2.6. *Rantamaa Formation (samples FI02006, FI02016, FI02020, and FI02021)*

The Rantamaa Formation is stratigraphically positioned at the top of the Kivalo Group of the Peräpohja Belt (Fig. 7) in northern Finland. It represents thick tidal flat successions of dolomitic carbonate with well-preserved stromatolitic and other supra- and synsedimentary intertidal structures (Lukkarinen and Lundqvist, 2000 and references therein). Our shale and dolomite samples were collected from the Louepalo quarry of the Tervola area in the Peräpohja Belt. Thin shale beds (cm scale) at this locality are intercalated with cm-scale beds of quartzite and dolomite; a sequence interpreted to represent deposition in a relatively calm shallow marine environment. Sulfide phases found in these samples include pyrite and chalcopyrite. The Rantamaa Formation overlies subaerial lavas of the Jouttiaapa Formation dated to 2.090 ± 0.070 Ga by the Sm-Nd method (Huhma et al., 1990). Rantamaa dolomites have highly positive $\delta^{13}C$ values, varying from +2.9 to +11.4‰ (Karhu, 1993) chemostratigraphically placing them toward the end of the major Paleoproterozoic global positive carbon isotope excursion, with a minimum age of 2.06 Ga (Karhu and Holland, 1996). During the Svecofennian orogeny at 1.9–1.8 Ga, the rocks of the Peräpohja Belt were folded and metamorphosed under lower greenschist facies conditions.

Three cubic grains of pyrite associated with phlogopite and microcrystalline dolomite in FI02006 (Fig. 8a) were found to have a range of $\delta^{34}S$ values >14‰ (between −1.20 and +13.13‰) and $\Delta^{33}S$ values between +0.00 and +0.08‰ (n = 3). The habits of pyrite grains in sample FI02016 are generally rounded subhedral to euhedral crystals found exclusively in bands of quartz and phlogopite either parallel to the sense of bedding or slightly discordant. Four of those grains (Fig. 8b) were analyzed by ion microprobe and found to have positive $\delta^{34}S$ values between +8.80 and +14.64‰ and $\Delta^{33}S$ values between −0.06 and +0.04‰ (n = 4). Sulfide phases of FI02020 include both pyrite and chalcopyrite disseminated in a matrix of small dolomite clasts. Three euhedral pyrite grains and one anhedral chalcopyrite bleb (Fig. 8c) have $\delta^{34}S$ values in the range of +7.68 to +9.42‰ and $\Delta^{33}S$ between −0.03 and −0.10‰ (n = 4). The phyllite FI02021 has small crystals and

Table 5. Electron microprobe analyses of sulfide grains from Paleoproterozoic sediments.

Sample grain[a]	Fe	S	Co	Ni	Cu	Zn	Total	Phase
FIK97-7b	44.39	52.55	0.1133	0.3641	0.0443	0.0154	97.47	Py
FIK97-7c	43.68	52.41	0.1080	0.8703	0	0.0127	97.07	Py
FIK97-11a	59.92	38.88	0.0223	0.2155	0.0143	0.0117	99.06	Po
FIK66-1a	59.47	38.40	0.1061	0.1246	0.0293	0	98.13	Po
FIK66-1b	59.19	37.86	0.1035	0.1335	0	0	97.28	Po
FIK66-1c	59.22	38.42	0.1078	0.1396	0.0191	0	97.91	Po
FIK118-2a	45.03	51.90	0.0839	0.0714	0	0.0389	97.12	Py
FIK119-8a	46.55	52.87	0.0579	0.0447	0	0	99.52	Py
FIK119-8b	45.97	52.30	0.0633	0	0	0	98.33	Py
FIK97-1b	47.89	46.64	0.0507	0	0	0.0497	94.63	Py
FIK97-1c	59.34	34.13	0.0561	0.0293	0.0316	0.0316	93.62	Po
FIK19-Aa	59.15	38.88	0.0736	0.0754	0	0	98.19	Po
FIK19-Ab	59.87	39.25	0.0534	0.1634	0	0	99.34	Po
FIK64-2a	60.00	39.62	0.1309	0.0625	0	0	99.81	Po
FIK64-2b	60.00	39.66	0.0977	0	0	0	99.76	Po
FI02006a	47.88	53.29	0.0500	0.0503	0	0	101.28	Py
FI02006b	46.98	51.75	0.0261	0.0103	0.0582	0	98.82	Py
FI02006c	46.77	54.12	0.0204	0.0025	0	0.0803	101.00	Py
FI02016a	46.27	53.36	0.1168	0.0573	0.0759	0	99.89	Py
FI02016b	46.23	53.55	0.0400	0	0.0075	0.0236	99.85	Py
FI02016c	46.75	54.54	0.0916	0.0452	0.0075	0.0079	101.44	Py
FI02016d	45.59	54.84	0.4246	0	0.0439	0	100.90	Py
FI02020a	46.55	54.27	0.1108	0.0336	0	0.0228	100.98	Py
FI02020b	45.72	54.9	1.0602	0	0	0.0340	101.71	Py
FI02020c	46.91	54.62	0.0668	0.0554	0	0	101.65	Py
FI02020d	29.26	35.01	0.0240	0	35.55	0.0241	99.87	Ch
FI02021b	30.16	35.84	0.0485	0	35.16	0	101.20	Ch
FI02021c	26.57	33.93	0.0294	0	28.82	0	89.35	Ch
FI02024a	47.47	54.51	0.1184	0	0	0.0102	102.11	Py
FI02024b	46.62	54.32	1.0154	0.0007	0.0272	0.0158	102.01	Py
FI02024c[b]	46.01	54.17	1.4048	0.0138	0	0.0167	101.61	Py
FI02024e	46.72	54.09	0.6726	0.0006	0.0521	0	101.54	Py
FI02025a	46.13	53.75	1.1254	0.0906	0.0385	0	101.14	Py
FI02025b	30.75	34.75	0.0086	0	26.92	0.0136	92.44	Ch
FI02025d	45.86	53.31	0.0681	0	0.4922	0.0094	99.73	Py
FI02026a	45.88	53.87	0.1738	0.4786	0.2531	0.0649	100.72	Py
FI02026b	46.83	54.11	0.0163	0.0113	0.0044	0	100.97	Py
FI02027a	47.06	54.09	0.0632	0.0227	0.0422	0	101.27	Py
FI02027b	46.70	54.21	0.2192	0.0260	0.0371	0	101.20	Py
FI02028b	47.23	53.94	0.1838	0.1881	0.0163	0	101.55	Py
FI02028c	46.96	54.37	0.0625	0.1670	0.0113	0.0662	101.64	Py
FI02031	37.13	53.96	0.0755	0.0746	0.0062	0	91.24	Py
FI02036a	46.32	54.00	0.0795	0.3519	0.0078	0	100.76	Py
FI02036b	46.03	53.86	0.0461	0	0.0931	0.0101	100.04	Py
FI02038a	47.42	53.99	0.0512	0.4637	0	0.0278	101.95	Py
FI02038b	46.78	53.92	0.0314	0.2561	0	0	100.98	Py
FI02040a	46.10	53.73	0.2042	0.0554	0	0.0151	100.10	Py
FI02041a	46.64	52.60	0.0752	0.0964	0.0150	0.0179	99.44	Py
FI02041b	46.83	53.08	0.2958	0.1947	0.0262	0.0057	100.43	Py
FI02043a	46.94	53.09	0.1082	0.3038	0.0077	0	100.45	Py
FI02043b	46.49	52.38	0.1421	0.2402	0	0.0058	99.26	Py
FI02043c	46.67	54.12	0.0966	0.2991	0.0407	0.0258	101.25	Py
FI02045a	46.52	55.11	0.5952	0.0547	0.0353	0.0239	102.34	Py
FI02045b	29.81	35.57	0.0475	0.0032	34.62	0.0946	100.15	Ch
FI112-NMK-96a	44.29	51.67	0.0328	0.0052	0.0479	0.0094	96.05	Py
FI112-NMK-96b	45.56	52.26	0.0428	0.0249	0	0	97.88	Py
FI112-NMK-96c	45.86	53.00	0.0500	0	0	0	98.91	Py
FI02052a	29.77	34.72	0.0405	0.0246	34.96	0.0358	99.55	Ch
FI02055a	45.68	52.34	1.3106	0.0008	0	0	99.33	Py
FI02055b	44.01	51.63	2.0978	0.0424	0	0	97.78	Py
GF7a	47.85	51.14	0.1412	0.0088	0.0174	0.0016	99.15	Py
GF7b	47.27	53.54	0.0168	0.0851	0	0.0125	100.92	Py
GF7c	46.66	53.90	0.0605	0.0733	0	0	100.70	Py
WY03010a	46.01	54.36	0.0953	0	0.0137	0	100.48	Py
PPRG1414a	46.36	51.89	0.0417	0.0648	0.0470	0	98.41	Py
PPRG1414b	47.41	53.37	0.0263	0	0	0.0122	100.82	Py
PPRG1414c	46.75	53.38	0.0443	0.0006	0	0	100.17	Py

[a] The code for the grain spot name is the sample number first, followed by a letter (a, b, c, or d) that identifies a different sulfide grain in the same sample.

[b] Data unavailable for FI02024d.

Table 6. SIMS sulfur isotopic analyses of sulfide grains from Paleoproterozoic sediments.

Grain spot*	^{34}S/^{32}S	±1σ	^{33}S/^{32}S	±1σ	^{32}S average intensity	δ^{34}S$_{CDT}$ (‰)	±2σ (‰)	δ^{33}S$_{CDT}$ (‰)	±2σ (‰)	Δ^{33}S (‰)	±2σ (‰)
January 2004 session											
FIK97-7b@1	4.376E-02	5.8E-07	7.871E-03	3.5E-07	1.30E+09	−9.01	0.67	−4.64	0.37	+0.04	0.13
FIK97-7c@1	4.376E-02	4.8E-07	7.871E-03	3.4E-07	1.24E+09	−9.05	0.67	−4.64	0.37	+0.06	0.13
FIK97-11a@1	4.359E-02	7.6E-07	7.854E-03	2.7E-07	9.86E+08	−13.07	0.67	−6.84	0.37	−0.05	0.12
FIK66-1a@1	4.441E-02	9.1E-07	7.932E-03	3.5E-07	9.77E+08	+5.66	0.67	3.04	0.37	+0.11	0.14
FIK66-1a@2	4.442E-02	6.3E-07	7.933E-03	4.8E-07	9.70E+08	+5.81	0.67	3.12	0.38	+0.12	0.15
FIK66-1b@1	4.440E-02	6.8E-07	7.930E-03	3.3E-07	9.65E+08	+5.31	0.67	2.75	0.37	0.00	0.13
FIK66-1c@1	4.442E-02	7.1E-07	7.933E-03	3.4E-07	9.88E+08	+5.94	0.67	3.18	0.37	+0.10	0.13
FIK118-2a@1	4.313E-02	6.7E-07	7.814E-03	2.8E-07	9.79E+08	−23.46	0.67	−11.92	0.37	+0.30	0.12
FIK118-2a@2	4.312E-02	7.0E-07	7.812E-03	2.5E-07	9.90E+08	−23.68	0.67	−12.09	0.37	+0.24	0.12
FIK119-8a@1	4.380E-02	5.2E-07	7.875E-03	2.5E-07	1.35E+09	−8.27	0.67	−4.21	0.37	+0.08	0.12
FIK119-8b@1	4.373E-02	6.7E-07	7.868E-03	2.9E-07	1.30E+09	−9.75	0.67	−5.03	0.37	+0.04	0.13
FIK97-1b@1	4.402E-02	6.2E-07	7.895E-03	3.2E-07	1.28E+09	−3.19	0.67	−1.60	0.37	+0.05	0.13
FIK97-1c@1	4.403E-02	8.4E-07	7.895E-03	3.1E-07	9.71E+08	−3.08	0.67	−1.59	0.37	+0.01	0.12
FIK19-Aa@1	4.381E-02	8.1E-07	7.875E-03	4.2E-07	9.03E+08	−8.00	0.67	−4.20	0.38	−0.05	0.15
FIK19-Aa@2	4.382E-02	6.9E-07	7.877E-03	3.8E-07	9.10E+08	−7.76	0.67	−3.93	0.37	+0.09	0.13
FIK19-Ab@1	4.384E-02	6.7E-07	7.878E-03	3.8E-07	9.03E+08	−7.20	0.67	−3.73	0.37	+0.01	0.14
FIK64-2a@1	4.381E-02	3.7E-07	7.876E-03	2.8E-07	1.00E+09	−8.03	0.67	−3.97	0.37	+0.19	0.12
FIK64-2a@2	4.383E-02	7.8E-07	7.877E-03	3.1E-07	1.00E+09	−7.59	0.67	−3.90	0.37	+0.04	0.13
FIK64-2b@1	4.385E-02	6.5E-07	7.880E-03	3.2E-07	1.01E+09	−7.01	0.67	−3.54	0.37	+0.10	0.13
FIK64-2b@2	4.385E-02	6.0E-07	7.879E-03	3.3E-07	9.90E+08	−7.18	0.67	−3.65	0.37	+0.08	0.13
FI02006a@1	4.457E-02	2.1E-06	7.946E-03	2.8E-07	1.31E+09	+9.32	0.68	+4.82	0.37	0.00	0.12
FI02006b@1	4.411E-02	1.8E-06	7.904E-03	3.9E-07	1.30E+09	−1.20	0.68	−0.54	0.38	+0.08	0.12
FI02006c@1	4.474E-02	6.8E-07	7.962E-03	3.6E-07	1.29E+09	+13.13	0.67	+6.86	0.37	+0.08	0.13
FI02016a@1	4.455E-02	8.1E-07	7.944E-03	2.3E-07	1.31E+09	+8.80	0.67	+4.57	0.37	+0.02	0.12
FI02016b@1	4.463E-02	1.1E-06	7.951E-03	3.0E-07	1.33E+09	+10.60	0.67	+5.49	0.37	+0.01	0.13
FI02016c@1	4.470E-02	7.8E-07	7.958E-03	3.0E-07	1.25E+09	+12.14	0.67	+6.31	0.37	+0.04	0.12
FI02016d@1	4.481E-02	1.2E-06	7.967E-03	2.0E-07	1.33E+09	+14.64	0.67	+7.49	0.37	−0.06	0.11
FI02020a@1	4.450E-02	6.3E-07	7.939E-03	2.6E-07	1.28E+09	+7.68	0.67	+3.94	0.37	−0.03	0.12
FI02020b@1	4.447E-02	6.7E-07	7.936E-03	2.3E-07	1.31E+09	+6.91	0.67	+3.50	0.37	−0.07	0.11
FI02020c@1	4.458E-02	3.8E-07	7.946E-03	2.6E-07	1.29E+09	+9.42	0.67	+4.76	0.37	−0.10	0.12
FI02020d@1	4.457E-02	6.1E-07	7.945E-03	2.9E-07	1.23E+09	+9.19	0.67	+4.69	0.37	−0.06	0.12
FI02021b@1	4.437E-02	5.6E-07	7.926E-03	2.3E-07	1.40E+09	+4.68	0.67	+2.35	0.37	−0.08	0.11
FI02021c@1	4.450E-02	1.1E-06	7.940E-03	4.0E-07	1.12E+09	+7.73	0.67	+4.00	0.38	0.00	0.14
FI02024a@1	4.457E-02	5.1E-07	7.946E-03	2.7E-07	1.32E+09	+9.27	0.67	+4.80	0.37	+0.01	0.12
FI02024b@1	4.458E-02	4.1E-07	7.947E-03	2.4E-07	1.33E+09	+9.52	0.67	+4.95	0.37	+0.03	0.12
FI02024b@2	4.458E-02	6.3E-07	7.947E-03	2.1E-07	1.31E+09	+9.52	0.67	+4.91	0.37	−0.01	0.11
FI02024c@1	4.453E-02	7.5E-07	7.942E-03	2.8E-07	1.35E+09	+8.41	0.67	+4.33	0.37	−0.01	0.12
FI02024d@1	4.414E-02	8.4E-07	7.907E-03	2.8E-07	1.29E+09	−0.45	0.67	−0.17	0.37	+0.06	0.12
FI02024e@1	4.450E-02	8.5E-07	7.939E-03	3.3E-07	1.34E+09	+7.62	0.67	+3.93	0.37	−0.01	0.13
FI02025a@1	4.440E-02	1.3E-06	7.930E-03	4.2E-07	1.38E+09	+5.36	0.67	+2.74	0.38	−0.03	0.13
FI02025b@1	4.444E-02	1.7E-06	7.933E-03	7.2E-07	5.22E+08	+6.20	0.68	+3.21	0.41	0.00	0.20
FI02025d@1	4.437E-02	4.8E-07	7.927E-03	2.3E-07	1.29E+09	+4.75	0.67	+2.47	0.37	+0.01	0.12
FI02026a@1	4.476E-02	1.0E-06	7.962E-03	3.0E-07	1.38E+09	+13.45	0.67	+6.85	0.37	−0.10	0.13
FI02026b@1	4.487E-02	9.0E-07	7.973E-03	3.4E-07	1.33E+09	+15.92	0.67	+8.19	0.37	−0.02	0.12
FI02026b@2	4.485E-02	5.8E-07	7.971E-03	1.7E-07	1.42E+09	+15.54	0.67	+8.03	0.36	+0.01	0.11
FI02027a@1	4.477E-02	8.3E-07	7.965E-03	2.0E-07	1.30E+09	+13.85	0.67	+7.19	0.37	+0.04	0.11
FI02027b@1	4.480E-02	7.5E-07	7.967E-03	2.6E-07	1.23E+09	+14.48	0.67	+7.42	0.37	−0.06	0.12
FI02028b@1	4.488E-02	1.4E-06	7.975E-03	2.4E-07	1.39E+09	+16.26	0.67	+8.48	0.37	+0.09	0.11
FI02028b@2	4.482E-02	5.0E-07	7.970E-03	2.2E-07	1.45E+09	+14.92	0.67	+7.80	0.37	+0.09	0.11
FI02028c@1	4.491E-02	3.6E-07	7.977E-03	2.4E-07	1.46E+09	+16.93	0.67	+8.71	0.37	−0.02	0.12
FI02028c@2	4.489E-02	1.0E-06	7.975E-03	2.7E-07	1.44E+09	+16.45	0.67	+8.50	0.37	+0.01	0.12
FI02031@1	4.466E-02	3.5E-07	7.955E-03	2.5E-07	1.30E+09	+11.30	0.67	+5.90	0.37	+0.06	0.12
FI02031@2	4.474E-02	5.9E-07	7.962E-03	3.0E-07	1.33E+09	+13.14	0.67	+6.80	0.37	+0.02	0.12
FI02031@3	4.465E-02	1.0E-06	7.953E-03	2.7E-07	1.32E+09	+11.14	0.67	+5.77	0.37	+0.01	0.12
FI02040a@1	4.476E-02	4.5E-07	7.963E-03	3.0E-07	1.36E+09	+13.60	0.67	+7.02	0.37	0.00	0.12
FI02041a@1	4.481E-02	6.7E-07	7.967E-03	2.8E-07	1.32E+09	+14.63	0.67	+7.45	0.37	−0.11	0.12
FI02041b@1	4.466E-02	8.0E-07	7.954E-03	3.2E-07	1.34E+09	+11.36	0.67	+5.84	0.37	−0.03	0.13
FI02043a@1	4.480E-02	7.0E-07	7.966E-03	3.2E-07	1.35E+09	+14.35	0.67	+7.36	0.37	−0.04	0.13
FI02043b@1	4.485E-02	4.3E-07	7.970E-03	2.6E-07	1.31E+09	+15.49	0.67	+7.92	0.37	−0.08	0.12
FI02043c@1	4.491E-02	5.2E-07	7.976E-03	1.7E-07	1.18E+09	+16.87	0.67	+8.66	0.36	−0.05	0.11
FI02045a@1	4.460E-02	7.6E-07	7.949E-03	2.4E-07	1.36E+09	+9.92	0.67	+5.16	0.37	+0.03	0.11
FI02045b@1	4.458E-02	1.3E-06	7.946E-03	3.1E-07	1.35E+09	+9.39	0.67	+4.77	0.37	−0.08	0.12
FIK112-NMK-96a@1	4.399E-02	6.1E-07	7.892E-03	4.4E-07	1.32E+09	−3.90	0.67	−1.96	0.38	+0.06	0.15
FIK112-NMK-96b@1	4.468E-02	6.7E-07	7.955E-03	2.2E-07	1.32E+09	+11.60	0.67	+6.00	0.37	0.00	0.11
FIK112-NMK-96c@1	4.471E-02	1.1E-06	7.958E-03	3.8E-07	1.32E+09	+12.45	0.67	+6.38	0.37	−0.05	0.13

Table 6. (Continued)

Grain spot*	$^{34}S/^{32}S$	$\pm 1\sigma$	$^{33}S/^{32}S$	$\pm 1\sigma$	^{32}S average intensity	$\delta^{34}S_{CDT}$ (‰)	$\pm 2\sigma$ (‰)	$\delta^{33}S_{CDT}$ (‰)	$\pm 2\sigma$ (‰)	$\Delta^{33}S$ (‰)	$\pm 2\sigma$ (‰)
FI02052a@1	4.437E-02	3.1E-06	7.927E-03	1.1E-06	3.58E+08	+4.77	0.69	+2.46	0.45	−0.01	0.25
FI02055a@1	4.368E-02	7.7E-07	7.864E-03	3.5E-07	1.29E+09	−10.88	0.67	−5.51	0.37	+0.14	0.14
FI02055b@1	4.374E-02	9.0E-07	7.869E-03	1.9E-07	1.22E+09	−9.49	0.67	−4.86	0.37	+0.07	0.11
GF7a@1	4.411E-02	7.0E-07	7.903E-03	2.8E-07	1.07E+09	−1.09	0.67	−0.57	0.37	−0.01	0.12
GF7a@2	4.412E-02	9.4E-07	7.905E-03	3.1E-07	1.06E+09	−1.06	0.67	−0.40	0.37	+0.15	0.12
GF7b@1	4.414E-02	4.3E-07	7.906E-03	3.3E-07	1.22E+09	−0.42	0.67	−0.23	0.37	−0.02	0.13
GF7c@1	4.414E-02	5.8E-07	7.906E-03	3.1E-07	1.25E+09	−0.43	0.67	−0.21	0.37	+0.01	0.12
WY03010a@1	4.413E-02	7.7E-07	7.905E-03	1.9E-07	1.34E+09	−0.79	0.67	−0.40	0.37	+0.01	0.11
June 2004 session											
FI02036a@1	4.509E-02	6.1E-07	7.967E-03	1.9E-07	7.18E+08	+21.10	0.63	+10.81	0.30	−0.06	0.10
FI02036a@2	4.509E-02	5.0E-07	7.965E-03	2.6E-07	7.23E+08	+20.92	0.63	+10.66	0.30	−0.12	0.12
FI02036a@3	4.509E-02	6.7E-07	7.966E-03	2.9E-07	7.31E+08	+21.00	0.63	+10.77	0.30	−0.06	0.12
FI02036b@1	4.496E-02	5.6E-07	7.955E-03	2.8E-07	7.40E+08	+18.00	0.63	+9.28	0.30	0.00	0.12
FI02036b@2	4.494E-02	8.6E-07	7.953E-03	3.1E-07	7.28E+08	+17.66	0.64	+9.10	0.30	−0.01	0.13
FI02038a@1	4.477E-02	6.5E-07	7.938E-03	2.7E-07	7.67E+08	+13.73	0.63	+7.15	0.30	+0.06	0.12
FI02038b@1	4.475E-02	5.6E-07	7.936E-03	3.2E-07	7.61E+08	+13.40	0.63	+6.93	0.30	+0.02	0.13
PPRG1414a@1	4.430E-02	6.6E-07	7.930E-03	4.0E-07	6.92E+08	+3.03	0.63	+6.13	0.31	+4.57	0.14
PPRG1414b@1	4.429E-02	5.8E-07	7.928E-03	2.9E-07	6.57E+08	+2.87	0.63	+5.93	0.30	+4.44	0.12
PPRG1414c@1	4.427E-02	8.8E-07	7.927E-03	4.3E-07	5.75E+08	+2.51	0.64	+5.77	0.31	+4.47	0.15

* The code for the name of the grain spot is the sample number first, followed by a letter (a, b, c or d) which identifies a different sulfide grain in the same sample, and @number (1, 2, or 3) which indicates the spot number on this sulfide grain.

large globules of chalcopyrite (hundreds of microns in size; Fig. 8d) with $\delta^{34}S$ values of +4.68 and +7.73‰ and these analyses indicated $\Delta^{33}S$ values of −0.08 and +0.00‰ respectively.

3.2.7. *Rantamaa Formation (samples FI02024, FI02025, FI02026, FI02027, FI02028, FI02031, FI02036, FI02038, FI02040, FI02041, FI02043, and FI02045)*

A section of the Rantamaa Formation is exposed in a quarry near Tervola, northern Finland. The section was mapped (Kortelainen, 1998) and systematically sampled over ~90 m; part of the section is shown in Figure 9. Preserved stromatolite features include flat laminations, domes and columns. Locally present are interlayers of siliciclastic units, interpreted as tidal channel deposits and storm layers. Sulfide phases found in these samples included both pyrite and chalcopyrite. The carbon and oxygen isotopes of the Rantamaa dolomite have been observed to negatively covary (Kortelainen, 1998) and in an effort to further investigate potential isotopic covariations, all samples from this sequence were analyzed for sulfur, carbon and oxygen isotopes.

A total of 12 samples from a section of the 2.06–2.09 Ga Rantamaa Formation were analyzed by ion microprobe. FI02024 was collected from position 90.0 m of the exposed section and consisted of dolomite with clasts of quartz, calcite and other minor phases including euhedral to subhedral pyrite crystals occurring throughout the matrix. Analyzed grains had $\delta^{34}S$ values between −0.45 and +9.52‰ and $\Delta^{33}S$ values varying between −0.01 and +0.06‰ (n = 6; Fig. 10a). The stromatolitic dolomite sample FI02025 was collected at 75.5 m and included randomly distributed subhedral pyrite and anhedral chalcopyrite grains (Fig. 10b). Sulfur isotopic compositions of these sulfides showed a small range in $\delta^{34}S$ values (between +4.75 and +6.20‰) and $\Delta^{33}S$ between −0.03 and +0.01‰ (n = 3). Two euhedral pyrite crystals from another stromatolitic dolomite FI02026 (collected at 69.1 m) were found to have heavy $\delta^{34}S$ values ranging from +13.45 to +15.92‰ and $\Delta^{33}S$ values between −0.10 and +0.01‰ (n = 3; Fig. 10c). Two euhedral pyrite crystals analyzed from the stromatolitic dolomite FI02027 (67.4 m; Fig. 10d) and duplicate analyses on two euhedral pyrite crystals in FI02028 (66.7 m; Fig. 10e) also revealed heavy $\delta^{34}S$ values (between +13.85 and +16.93‰) and $\Delta^{33}S$ values between −0.06 to +0.09‰ (n = 6 for both samples). The quartzite FI02031 (54.8 m; Fig. 10f) had a large (~1 cm) cubic pyrite crystal, on which triplicate ion microprobe analyses revealed $\delta^{34}S$ values between +11.30 and +13.14‰ and $\Delta^{33}S$ between +0.02 and +0.06‰. A dolomitic quartzite FI02036 (30.0 m; Fig. 10g) had few euhedral pyrite crystals, two of which were found to have $\delta^{34}S$ values between +17.66 and 21.10‰ and $\Delta^{33}S$ between −0.12 and +0.00‰. Two euhedral pyrite grains in FI02038 (2.0 m above FI02036) revealed $\delta^{34}S$ values of +13.40 and +13.73‰ and $\Delta^{33}S$ values of +0.02 and 0.06‰ respectively (Fig. 10h). A subhedral pyrite grain from the dolomitic quartzite FI02040 (25.0 m; Fig. 10i) was found to have a $\delta^{34}S$ value of +13.60‰ and a $\Delta^{33}S$ value of +0.00‰. Sample FI02041 was collected at position 20.0 m and is a microcrystalline dolomite rock with laminar stromatolite features. Two subhedral pyrites (Fig. 10j) had $\delta^{34}S$ values of +14.63 and +11.36‰ and $\Delta^{33}S$ values of −0.11 and −0.03‰, respectively. The stromatolitic dolomite FI02043 was collected at 11.0 m and had euhedral pyrite grains with $\delta^{34}S$ values between +14.35 and +16.87‰ and $\Delta^{33}S$ values between −0.04 and −0.08‰ (n = 3; Fig. 10k). Finally, pyrite and chalcopyrite were both recognized in the stromatolitic dolomite FI02045 (0.0 m) associated with quartz-rich layers. Two subhedral grains of pyrite and chalcopyrite had $\delta^{34}S$ values of +9.39 and +9.92‰ and $\Delta^{33}S$ values of −0.08 and +0.03‰ (Fig. 10l). The sulfur isotopic compositions of all the studied sulfide grains from the Rantamaa section show a range of ~22‰ in $\delta^{34}S$. The chemostratigraphic profile of sulfur

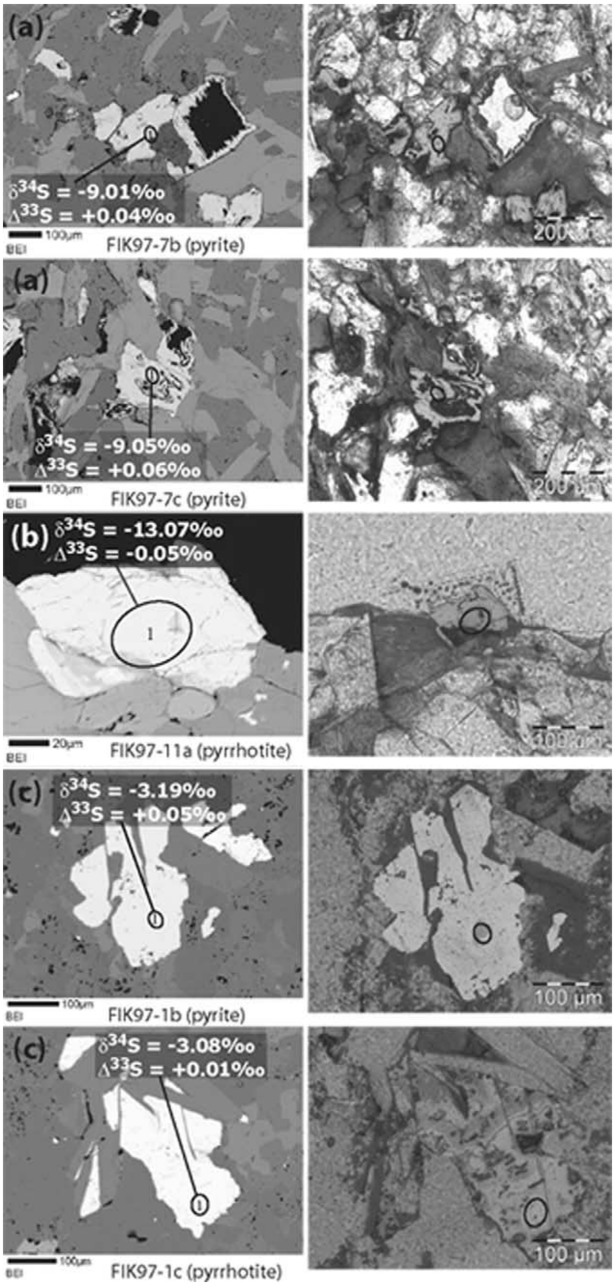

Fig. 4. BSE and transmitted/reflected light images of analyzed sulfide grains from Kainuu Belt (Fig. 1) with labeled ion microprobe spots. (a) Subhedral pyrite crystals from FIK97-7. (b) Analyzed subhedral pyrrhotite grain in FIK97-11. (c) Subhedral pyrite and pyrrhotite grains from FIK97-1.

isotopes in the measured Rantamaa section was also studied for carbon and oxygen isotope fractionations to identify potential isotopic covariations. Results of isotopic analyses on the Rantamaa carbonates are shown in Table 7 and plotted in Figure 11 along with the $\delta^{34}S$ and $\Delta^{33}S$ values. The $\delta^{18}O_{carb}$ values were relatively low and varied between −9.99 and −6.78‰. These carbonates were also characterized by a small range of $\delta^{13}C_{carb}$ values between +3.28 to +4.79‰.

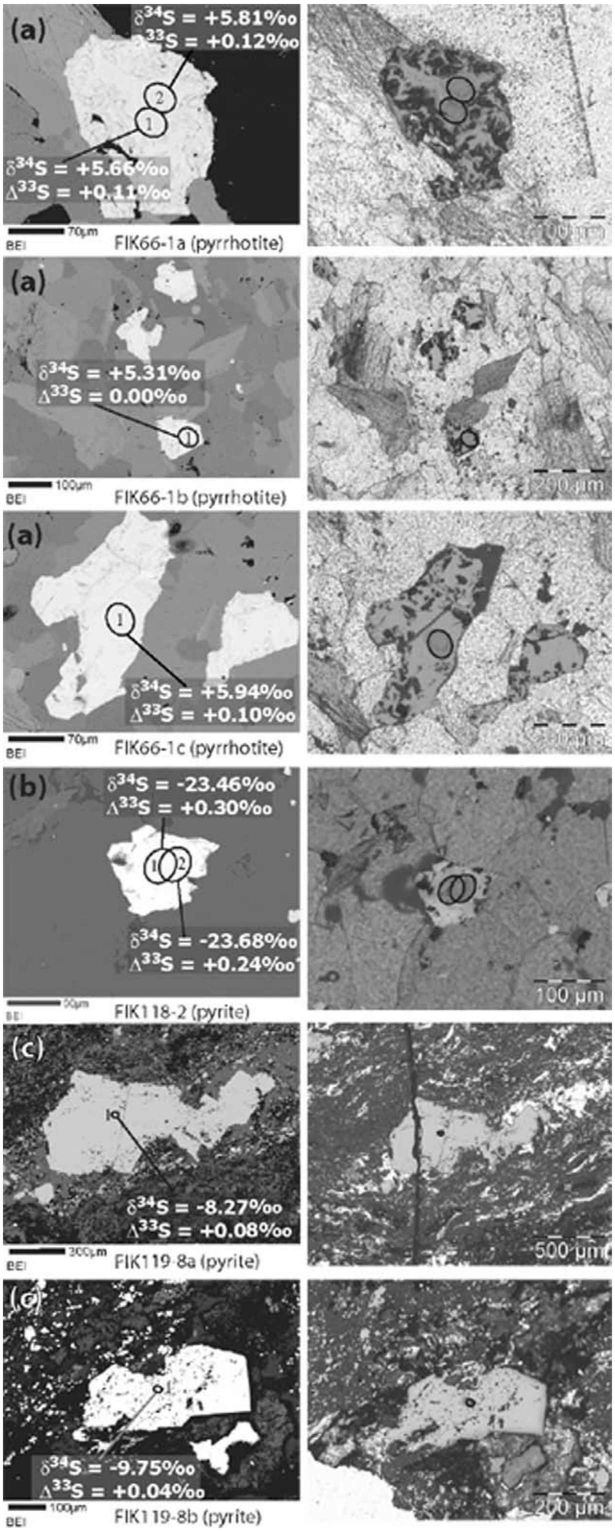

Fig. 5. BSE and transmitted/reflected light images of sulfides from Outokumpu schist and Outokumpu Association (Fig. 1) indicating multiple sulfur isotopic composition of ion microprobe spots. (a) Three pyrrhotite grains from FIK66-1. (b) Two sulfur isotopic analyses of anhedral pyrite grain from FIK118-2. (c) Subhedral pyrite crystals from FIK119-8.

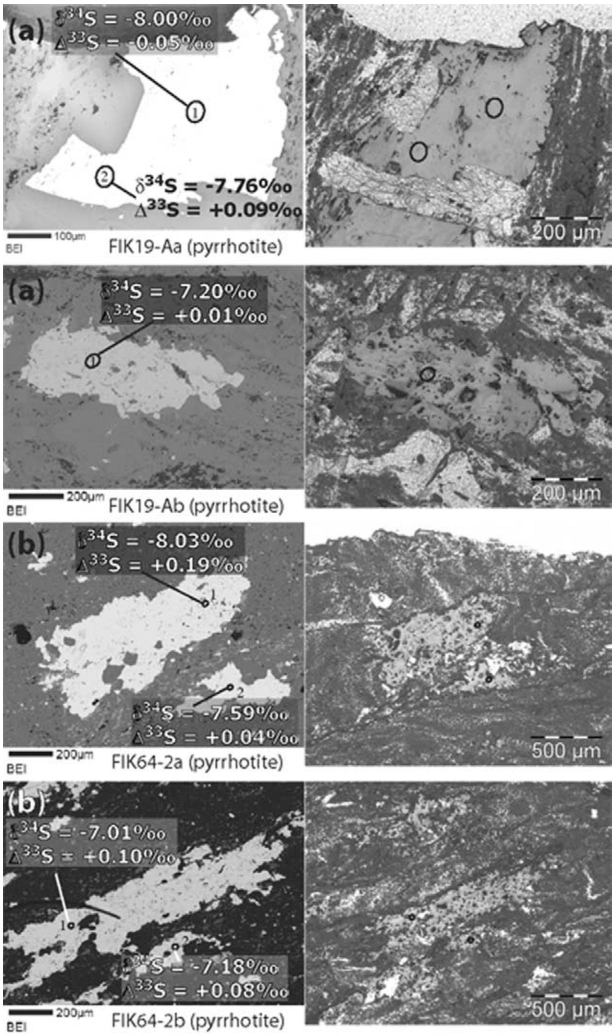

Fig. 6. BSE and transmitted/reflected light images of sulfides from Mulo area and Kittilä Group (Fig. 1) labeled with delta values of ion microprobe spot. (a) Subhderal and anhedral pyrrhotite grains in sample FIK19-A. (b) Large anhedral pyrrhotite grains from sample FIK64-2.

3.2.8. *Rantamaa Formation (sample FI112-NMK-96)*

A section of the Rantamaa Formation is exposed ~7 km east from the Rantamaa Quarry. The sequence is lithologically similar and considered to be correlative to that exposed in the quarry. Stromatolite features are well-preserved and interlayers of siliclastic units are present locally. Quartzite sample FI112-NMK-96 contains dolomite disseminated in a quartz matrix with many large (mm size) euhedral pyrite crystals (Fig. 12a). Sulfur isotopic analyses revealed a 16‰ range of δ^{34}S values (between −3.90 and +12.45‰) and Δ^{33}S values between −0.05 and +0.06‰ (n = 3).

3.2.9. *Sompujärvi Formation (samples FI02052 and FI02055)*

The Sompujärvi Formation in Finland consists mostly of quartzite with arkosic and schist interbeds. The formation represents the lowermost supracrustal unit of the Peräpohja schist belt, overlying the 2.7 Ga Archean basement and 2.43 Ga layered intrusions (Perttunen and Vaasjoki, 2001). A minimum age for the Sompujärvi Formation is set by the numerous 2.20–2.22 Ga diabase sills and dykes intruding the overlying sedimentary units of the Palokivalo Formation (Perttunen and Vaasjoki, 2001). Our samples FI02052 and FI02055 were collected 3.9 and 10.1 m above the unconformity contact with the Archean basement and sulfide phases present in these sediments include chalcopyrite and pyrite. Figure 7 shows the geological context of the Sompujärvi Formation in the Kivalo Group of the Peräpohja Belt.

A 2.22–2.43 Ga quartzite schist FI02052 was found to have chalcopyrite associated with hornblende. Analysis of a chalcopyrite bleb (Fig. 12b) revealed a δ^{34}S value of +4.77‰ and Δ^{33}S value of −0.01‰. For an undetermined reason, this analysis had a ^{32}S-intensity about three times less than the average for chalcopyrite (Table 6 and Fig. 5). The quartzite schist FI02055 is rich in biotite and has a group of relatively large euhedral to subhedral pyrite crystals associated with hornblende and prehnite. Two grains were found to have negative δ^{34}S values of −9.49 and −10.88‰ and Δ^{33}S values of +0.07 and +0.14‰ respectively (Fig. 12c).

3.2.10. *Gunflint Formation (sample GF7)*

A zircon U-Pb age of 1.878 Ga was determined for tuffaceous layers of the Gunflint Formation (Fralick et al., 2002). The Gunflint Formation is known to have relatively high concentrations of organic matter with $\delta^{13}C_{org}$ values down to −34‰ in chert (Strauss and Moore, 1992) and whole-rock δ^{34}S values around −1‰ for an associated iron formation (Cameron and Garrels, 1980). GF7 is a microfossiliferous stromatolitic

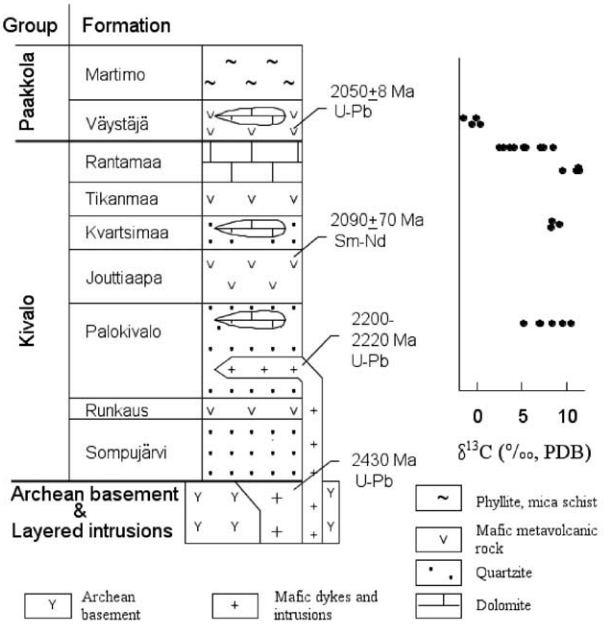

Fig. 7. Generalized stratigraphy of Paleoproterozoic Peräpohja Belt, northern Finland. Variation in δ^{13}C compositions of sedimentary carbonates is shown after Karhu (1993, 2005).

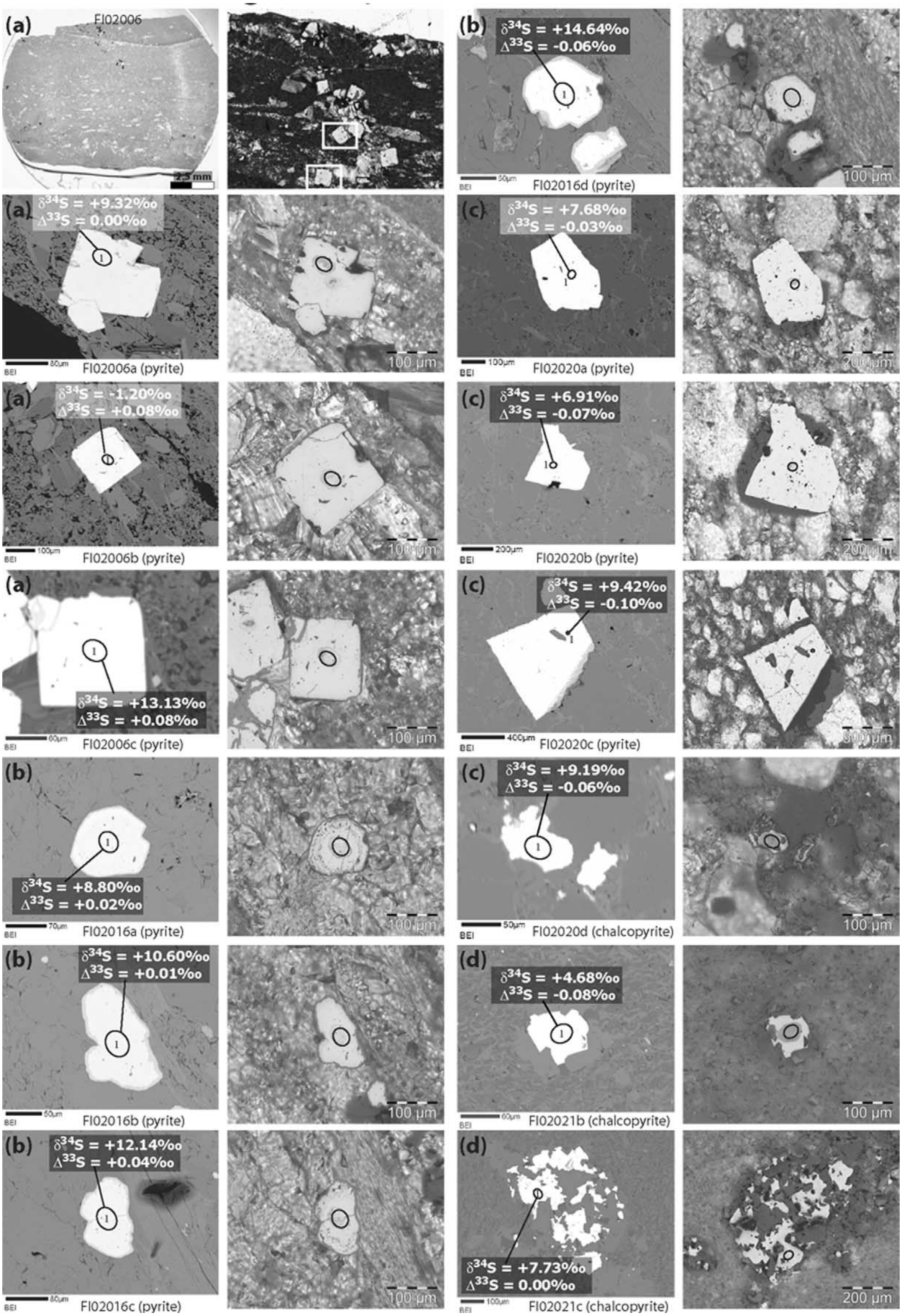

Fig. 8. BSE and transmitted/reflected light images of sulfides from Rantamaa Formation showing sulfur isotopic composition of ion microprobe spot. (a) Thin section of FI02006 and blown-up view of pyritiferous region where three euhedral pyrite crystals were analyzed. (b) Four rounded euhedral pyrite grains from FI02016. (c) Three pyrite and one chalcopyrite grains analyzed from FI02020. (d) Two blebs of chalcopyrite analyzed in FI02021.

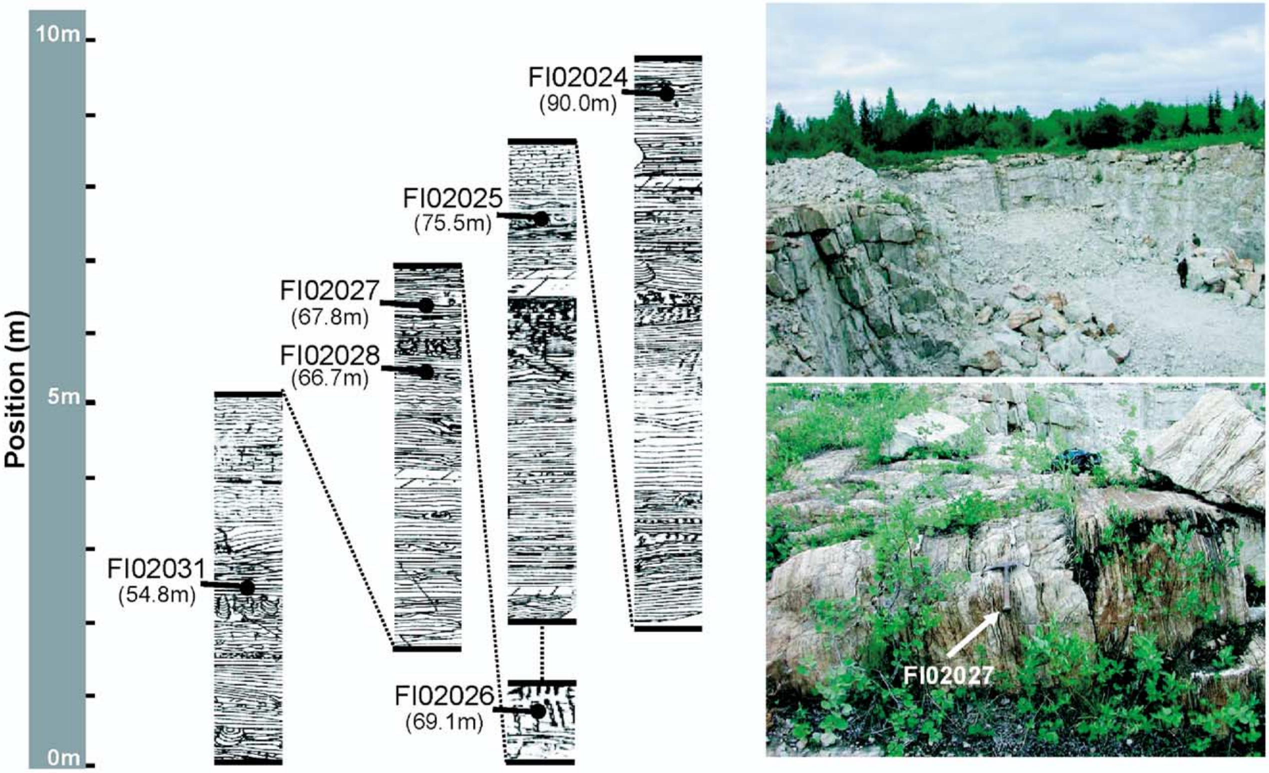

Fig. 9. Stratigraphy (based on Kortelainen, 1998) and field images of Rantamaa quarry and sampled section of Rantamaa Formation (northern Finland). Sampled dolomites occur as columnar or laminated stromatoforms; location of several samples analyzed in this study is shown in stratigraphic context.

black chert (Barghoorn and Tyler, 1965) collected from the Schreiber locality, in Ontario (Canada), which includes multiple euhedral pyrite crystals as well as a few concentric globules with pyritic rims (Fig. 13a). Our isotopic analyses of three pyrite grains revealed a small range of δ^{34}S values between -1.09 and -0.42‰ and Δ^{33}S values between -0.02 and $+0.15$‰ ($n = 4$).

3.2.11. *Nash Fork Formation (sample WY03010)*

The Nash Fork Formation is part of the Upper Libby Creek Group and stratigraphically overlies the three glacial diamictites of the Snowy Pass Supergroup of southern Wyoming. It is dominantly massive and stromatolitic dolomite generally characterized by high $\delta^{13}C_{carb}$ values and layers of argillite that contain sulfate molds (Bekker et al., 2003a). Chemostratigraphy based on $\delta^{13}C_{carb}$ values can been used to estimate the age of the Nash Fork Formation between ~2.25 and 2.05 Ga. The Libby Creek Group in Wyoming was metamorphosed to greenschist facies during the 1.74–1.78 Ga Medicine Bow orogeny (Chamberlain, 1998). WY03010 is an argillite containing vugs probably from the dissolution of gypsum crystals. A few small pyrite grains are associated with dolomite crystals that appear to have refilled some gypsum molds. A euhedral grain ~90 μm in size had a rim of iron oxide surrounding an irregularly shaped core (~60 μm in size) of pyrite. The core was found to have a δ^{34}S value of -0.79‰ and a Δ^{33}S value of $+0.01$‰ (Fig. 13b). The high spatial resolution provided by coupled electron and ion microprobe techniques is well demonstrated by this type of analysis.

3.2.12. *Gamohaan Formation (sample PPRG1414)*

The Gamohaan Formation is part of the Campbellrand subgroup of the Transvaal Supergroup in South Africa and contains sediments deposited in a shallow marine environment. The Gamohaan Formation has a U-Pb zircon age of 2.516 ± 0.004 Ga determined from tuff beds in the upper parts of the formation (Altermann and Nelson, 1998). Sample PPRG1414 is a bedded black chert collected by J. W. Schopf. Black cherts from the Gamohaan Formation contain organic carbon with δ^{13}C values varying between -37.4 and -33.2‰, which points to a biologic origin for the carbon (Strauss and Moore, 1992). Sulfides in PPRG1414 are present as small grains of pyrite with an average size around 30 μm. Three euhedral to anhedral pyrites from PPRG1414 were analyzed during the June 2004 session and found to have δ^{34}S values between $+2.51$ and $+3.03$‰ and Δ^{33}S values between $+4.44$ and $+4.57$‰ (Fig. 13c).

4. DISCUSSION

4.1. Sources of Sulfur in Sediments

Sulfur is widely distributed in the Earth and occurs in oxidized forms (sulfate), neutral state (elemental S^0) and reduced

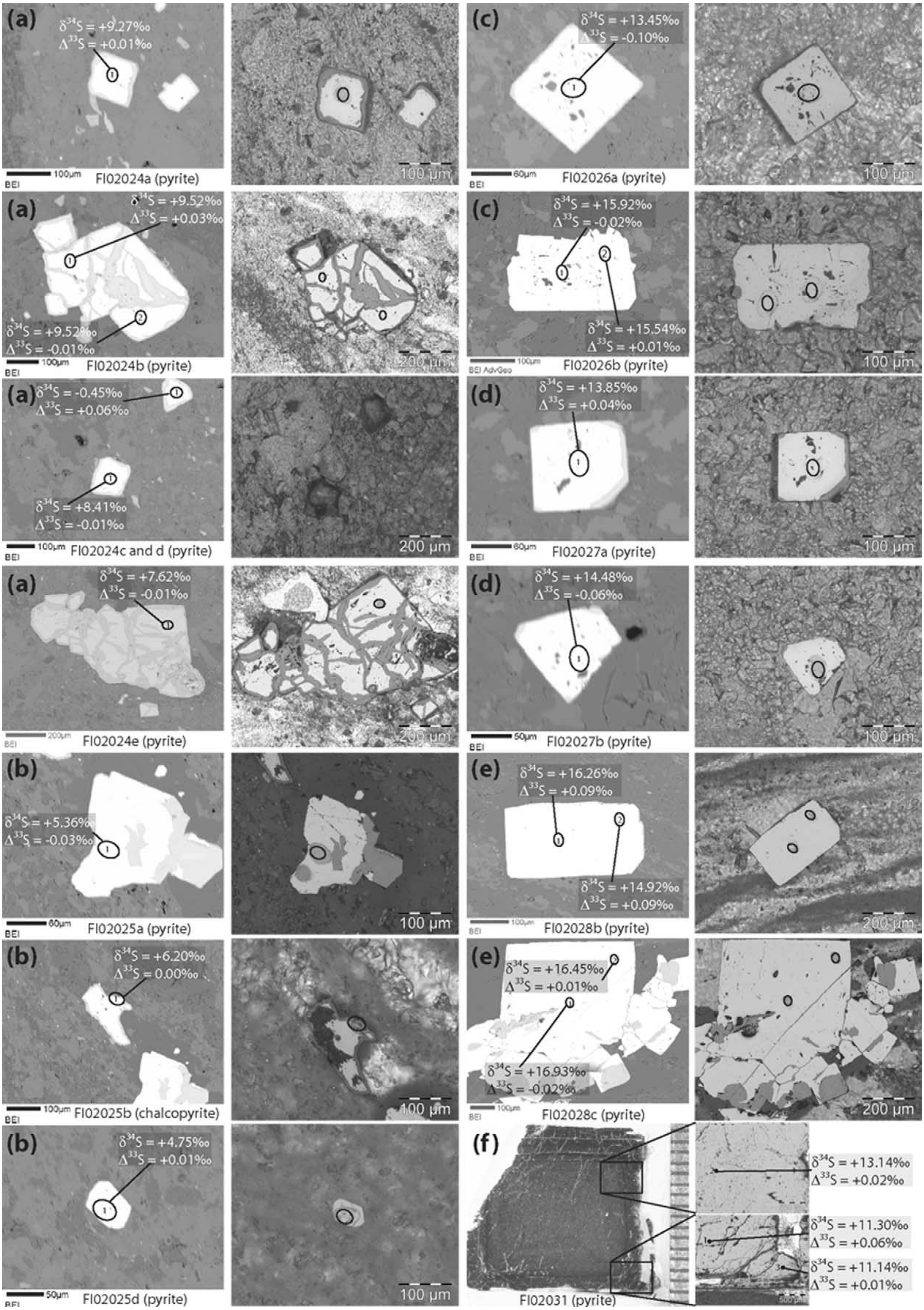

Fig. 10. Please see legend on next page.

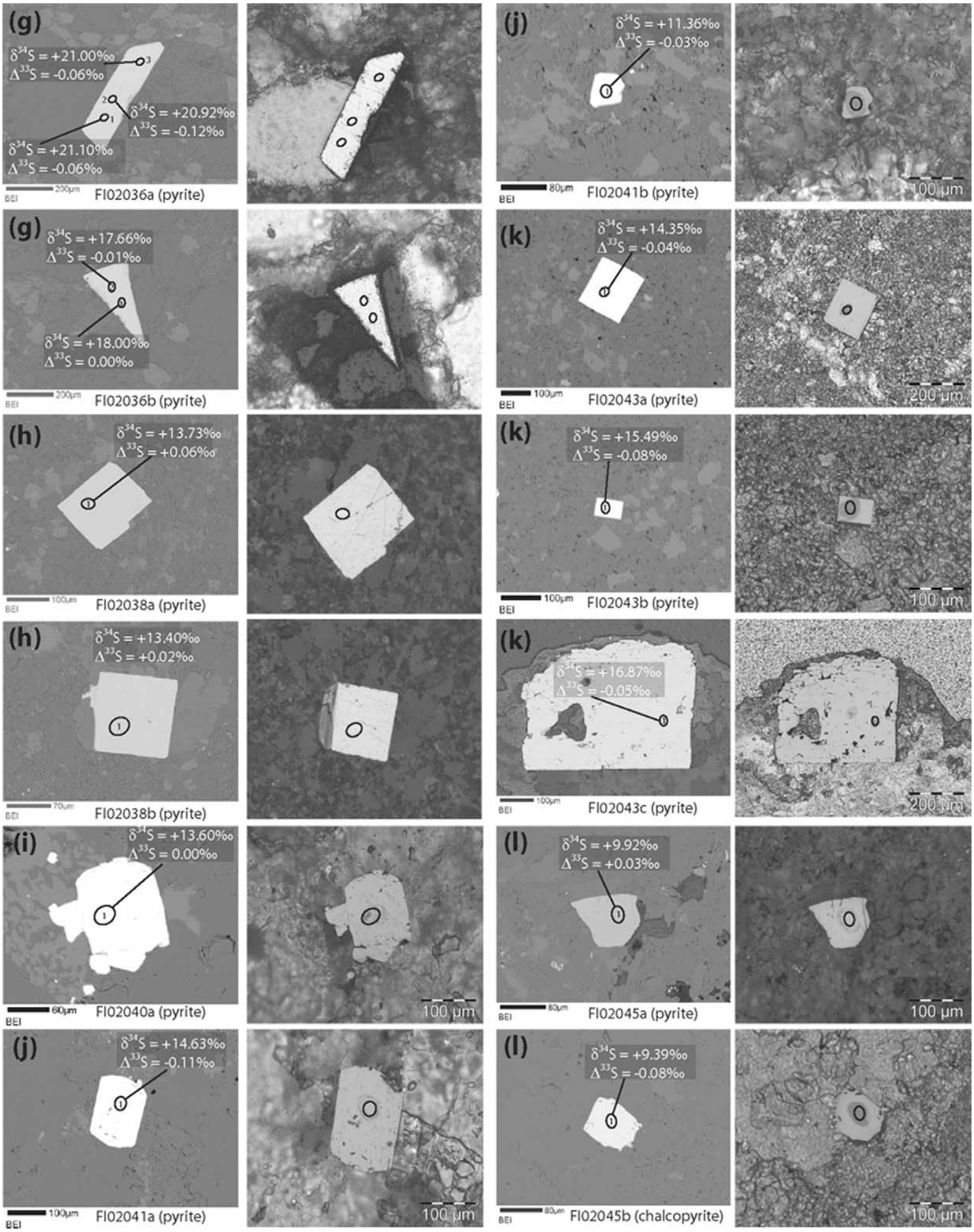

Fig. 10. BSE and transmitted/reflected light images of sulfide grains from section of Rantamaa Formation indicating delta values of analyzed ion microprobe spots. (a) Five pyrite grains from FI02024 with noticeable Fe-oxide edges (grains FI02024c and d were lost during cleaning after ion microprobe analysis). (b) Three sulfide grains from FI02025. (c) Two euhedral pyrite grains analyzed in FI02026. (d) Two analyzed pyrite crystals from FI02027. (e) Two analyzed euhedral pyrite crystals from FI02028. (f) Three ion microprobe analyses of large euhedral pyrite crystal in FI02031. (g) Two euhedral pyrite grains from FI02036. (h) Two euhedral pyrite crystals from FI02038. (i) Euhedral pyrite grain from FI02040. (j) Two subhedral pyrite crystals analyzed in FI02041. (k) Three cubic pyrite crystals analyzed in FI02043. (l) Two anhedral grains of pyrite and chalcopyrite from FI02045.

Table 7. Chemostratigraphic data for the measured section of the Rantamaa Formation.

Sample (position)	$\delta^{13}C_{PDB}$ (‰)	$\delta^{18}O_{v\text{-}smow}$ (‰)
FI02024 (90.0m)	+4.79	−8.46
FI02025 (75.5m)	+3.82	−7.78
FI02026 (69.1m)	+4.06	−7.53
FI02027 (67.8m)	+4.16	−7.42
FI02028 (66.7m)	+4.39	−7.37
FI02036 (30.0m)	+4.54	−9.99
FI02038 (28.0m)	+4.10	−9.37
FI02040 (25.0m)	+3.94	−9.00
FI02041 (20.0m)	+3.78	−7.63
FI02043 (11.0m)	+3.59	−6.78
FI02045 (0.0m)	+3.28	−7.05

forms (sulfides). Detrital sulfides, which can sometimes be identified from their rounded appearance and occurrence with other characteristic detrital minerals, are older than the depositional age of the sediment. Sulfide formation can postdate the origin of host sedimentary rocks if they formed from the crystallization of remobilized sulfur from fluids. Criteria used to distinguish sedimentary from hydrothermal sulfides include the sulfur isotopic composition and sometimes an unusual abundance of trace metals. However, hydrothermal fluids may assimilate sulfur from host sedimentary rocks during water-rock interactions and therefore carry the $\delta^{34}S$ value of the host rock. For instance, pyrite in sediments may have the isotopic signature of microbial sulfate reduction and subsequent hydrothermal circulation can transport Cu that will react with pyrite to form chalcopyrite with the same $\delta^{34}S$ as the precursor pyrite (Ohmoto and Goldhaber, 1997). Chalcopyrite in samples FI02020 and FI02021 could have formed in this manner by the replacement of preexisting pyrite during metamorphism, and hence the $\delta^{34}S$ should be the same as that of the precursor sulfide. High concentrations of trace metals such as Co, Zn and Ni in sulfides may also be indicative of diagenetic conditions or interaction with magmatic or other fluids (Ohmoto and Goldhaber, 1997). Some pyrite crystals in samples FIK97-7 and FI02026 have relatively high Ni contents (1% > [Ni] > 0.35%; Table 5) and pyrite grains from FI02020, FI02024, FI02025 and FI02055 have high Co contents (2.1% > [Co] > 1.0%; Table 5), which may indicate euxinic conditions during deposition and/or postdiagenetic interaction with fluids. The $\delta^{34}S$ value of sulfur in igneous rocks from the upper mantle is in the range of −0.7 ± 5.0‰ (Chaussidon and Lorand, 1990) and more generally is in the range of −3.0 to +3.0‰ (Ohmoto, 1986). Sulfur isotopes of magmas will have $\Delta^{33}S$ values equal to 0‰, unless the magma originated primarily from recycled Archean sediments with a nonzero $\Delta^{33}S$ and the MIF sulfur

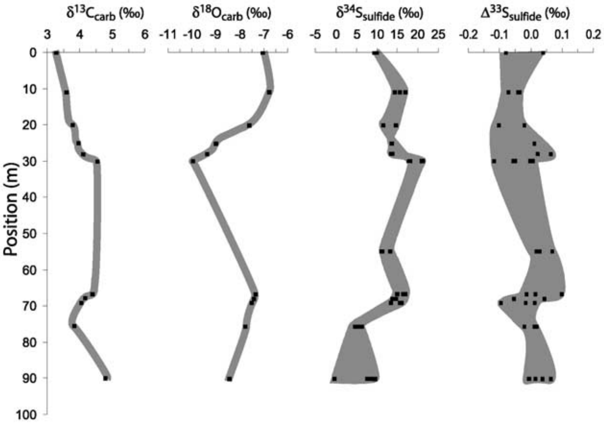

Fig. 11. Chemostratigraphic profile of $\delta^{13}C_{carb}$, $\delta^{18}O_{carb}$, $\delta^{34}S_{sulfide}$, and $\Delta^{33}S_{sulfide}$ in section of Rantamaa Formation exposed in quarry.

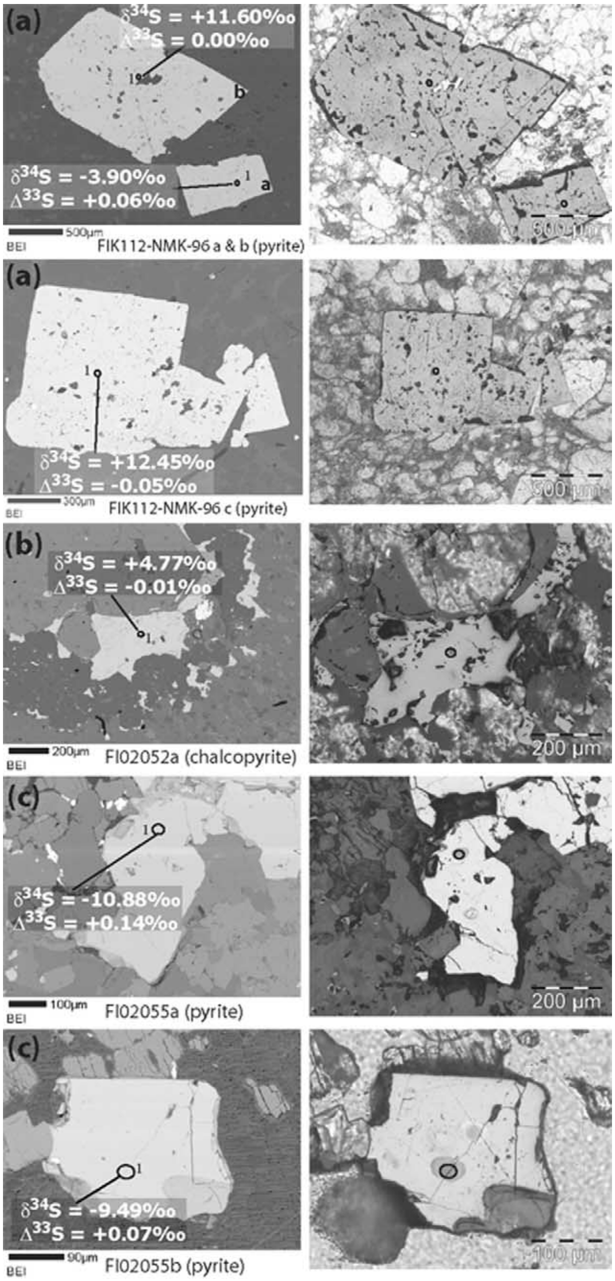

Fig. 12. BSE and transmitted/reflected light images of sulfide grains from Rantamaa and Sompujärvi Formations showing labeled ion microprobe spots. (a) Three large euhedral pyrite crystals from FI112-NMK-96. (b) Crystal of chalcopyrite analyzed from FI02052. (c) Two pyrite grains analyzed from FI02055.

isotopes were isolated from dilution by mantle sulfur (e.g., Farquhar et al., 2002).

Metamorphism only slightly fractionates sulfur isotopes and these minor fractionation effects are mass-dependent. Metamorphic events can potentially modify the Δ^{33}S value of sedimentary sulfides but this can only be achieved by interaction with sulfur-containing metamorphic fluids such that a preexisting MIF signature is either diluted or remobilized. Near-zero Δ^{33}S values do not necessarily imply high levels of atmospheric O_2 at time of deposition; MIF sulfur isotopes can readily be diluted by MDF sulfur. This argument probably explains the observation that some sulfides with nonzero Δ^{33}S values from Archean sediments occur in samples that also have MDF sulfur isotopes (Farquhar et al., 2000; Hu et al., 2003; Mojzsis et al., 2003). It is important to emphasize that the presence of a MIF sulfur isotopic signature is consistent with sedimentary sulfur that cycled through the atmosphere. However, to propose that MIF sulfur isotopes were absent at time of deposition requires other lines of evidence such as δ^{34}S, sulfide composition, morphology and petrogenesis that indicate a sedimentary source of sulfur. Most sulfides from ~1.9 to 2.1 Ga sediments analyzed in this study have δ^{34}S values that are broadly in agreement with a sedimentary sulfur source (sec. 3.2). Thus the most straightforward interpretation is that Δ^{33}S signatures reported here indicate that atmospheric O_2 levels were consistently well above the canonical ca. 10^{-5} PAL pO_2 value at time of deposition. On the other hand, the source of sulfur in samples for which sulfides have δ^{34}S values that overlap the igneous range ($-0.7 \pm 5.0‰$) is uncertain. Our δ^{34}S values for pyrrhotite from FIK66-1 (around +5 to +6‰) are close to the range of igneous values so that the near-zero Δ^{33}S values for these sulfides may not necessarily represent environmental conditions at time of deposition. Similarly, the origin of the sulfur isotopic signatures in FI02025, FI02052, GF7 and WY03010 is ambiguous because their δ^{34}S values do not necessarily support a sedimentary origin for the Δ^{33}S. Therefore without more data to support a sedimentary source of sulfur, the near-zero Δ^{33}S values of these samples cannot be used to constrain atmospheric O_2 at time of deposition.

The shapes of the analyzed sulfide crystals vary from anhedral to euhedral and may be related to degree of recrystallization related to, e.g., metamorphism. All sediments analyzed in this study experienced lower greenschist to amphibolite facies metamorphism, which likely modified the original sulfide grain morphologies. Analysis of BSE and reflected light images in this study fail to show any obvious correlations between sulfur isotopic composition and grain shape. Therefore we would argue that the habit of a sulfide grain is a weak criterion to assess the sedimentary origin of the sulfur, unless specific features can be identified such as sulfide nodules. Metamorphic recrystalization is probably responsible for most of the large cubic and euhedral crystals observed in our samples and the

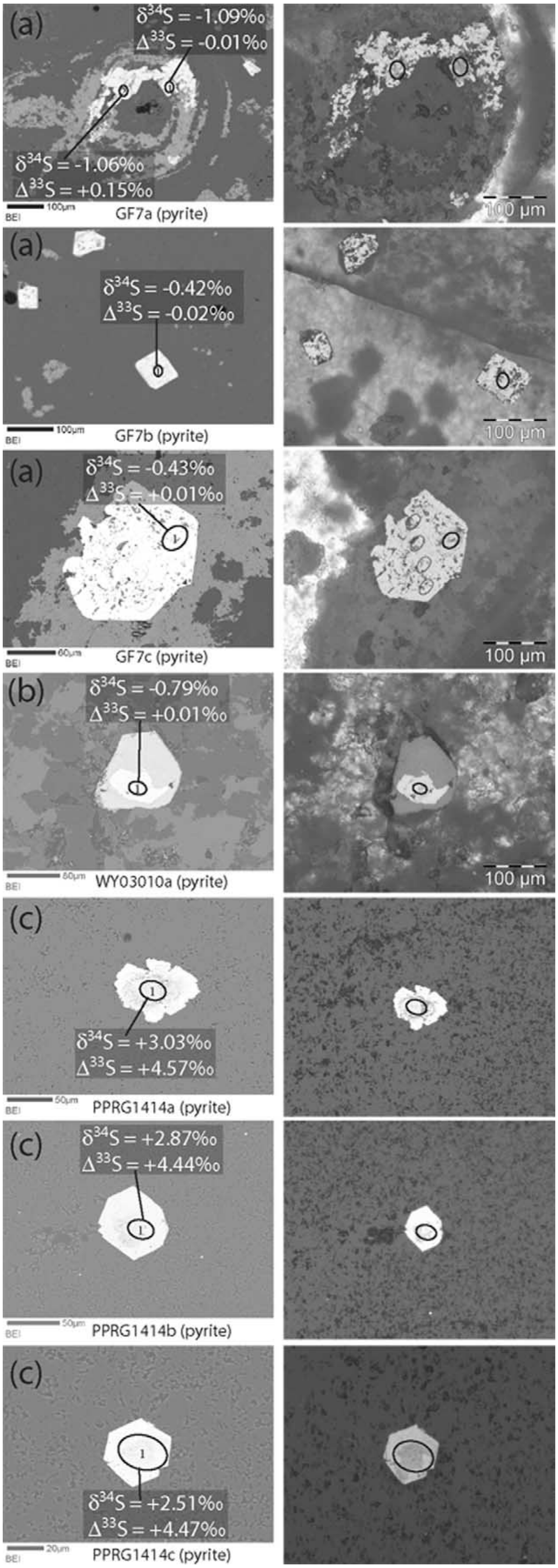

Fig. 13. BSE and transmitted/reflected light images of sulfide grains from Gunflint and Nash Fork Formations indicating analyzed spots with their delta values. (a) Thin section of GF7 with location of pyrite globule and two euhedral pyrite grains. (b) Partially oxidized anhedral pyrite core in subhedral Fe-oxide grain in WY03010. (c) Three small pyrite grains analyzed in PPRG1414.

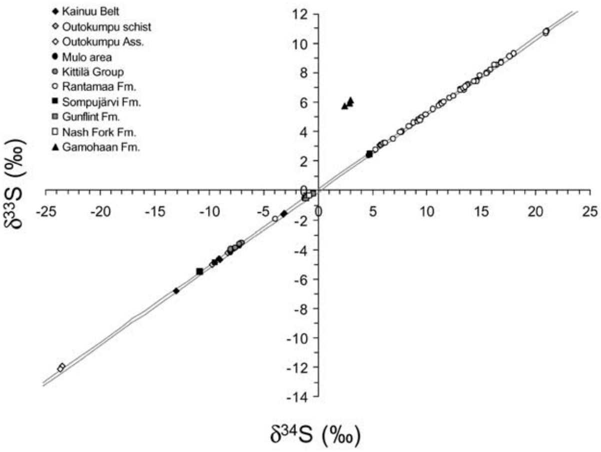

Fig. 14. Three-isotope plot of data for sulfides analyzed in January 2004 and June 2004 sessions. Gray lines are limits of York-MDF band for January standards, which are identical to those for June standards.

BSE and reflected light images do not show any obvious evidence for sulfide overgrowths on preexisting sulfide cores.

4.2. Multiple Sulfur Isotope Fractionation in Natural Samples

As outlined above (sec 3.1), comparison of our results for sulfur isotopes on a three-isotope plot can be done using the MDF band defined by the regression of our standards. Figure 14 shows that most analyses fall within the MDF band, but that a few data lie outside, although very close to the band. This is the case of the duplicate analyses on FIK118-2, measured to have $\Delta^{33}S$ values of $+0.30$ and $+0.25$‰, which may arise from a combination of kinetic and equilibrium reactions leading to different MDF effects (Young et al., 2002). Because these data are consistent with microbial sulfate reduction (pyrite in FIK118-2 has $\delta^{34}S \sim -24$‰) an apparent small departure from MDF is possible. Similarly negative $\delta^{34}S$ values for biogenic pyrite nodules from the Timeball Hill Formation in South Africa were also characterized by a small shift from MDF with $\Delta^{33}S$ values of up to $+0.33$‰ (Bekker et al., 2004). These observations in natural samples could be interpreted by analogy with experiments using the sulfate reducing archeon *Archaeglobus fulgidus* in which the sulfur isotopes are slightly off the strict MDF line (but within our York-MDF regression band) with $\Delta^{33}S$ between -0.05 and $+0.07$‰ and where $\lambda = 0.5117$ for $\delta^{34}S$ values between about -21 and $+16$‰ (Farquhar et al., 2003). This interpretation may also apply to pyrites in FI02055 and FIK64-2, which are seen in Figure 14 to fall somewhat outside the York-MDF band. These data therefore contribute useful evidence for exploring naturally-occurring small deviations (e.g., $\Delta^{33}S < 0.35$‰) from strict MDF imparted by microbial sulfate reduction.

4.3. Paleoproterozoic Glaciations and the Demise of MIF

Organic biomarkers suggest the existence of oxygenic photosynthesis and eukaryotes by 2.7 Ga (Brocks et al., 1999) and indicate at least that the potential for traces of atmospheric O_2 could have existed at that time. Our data indicate a large MIF sulfur isotopic signature in pyrite from the 2.516 Ga black chert of the Gamohaan Formation with positive $\Delta^{33}S$ values around $+4.5$‰, which clearly indicates a sedimentary source of sulfur and independently confirm the results of Farquhar et al. (2000) for the same formation. The Mt. McRae shale in the Hamersley Group of Western Australia was deposited around the same time and was found to have $\Delta^{33}S$ values up to $+6.9$‰ (Ono et al., 2003). Such high $\Delta^{33}S$ values are thoroughly consistent with our results for the Gamohaan Formation and imply an anoxic atmosphere at the beginning of the Paleoproterozoic.

Positive $\Delta^{33}S$ values in sulfides may be preserved by the activity of microbial elemental sulfur reduction after cycling in the atmosphere (Farquhar et al., 2001; Mojzsis et al., 2003), but we note that the small range of $\delta^{34}S$ values for the Gamohaan sulfides cannot be used to evaluate this. Global mafic magmatism between ~2.48 and 2.42 Ga has been interpreted to be related to the breakup of a Late Archean supercontinent (Heaman, 1997). Enhanced tectonic activity at the beginning of the Paleoproterozoic is likely to have resulted in increased weathering of continental crust. We propose that increased erosion rates at that time would have led to increased nutrient (e.g., phosphate) delivery to the oceans by rivers. These favorable conditions for microbial communities resulted in increased primary productivity (e.g., oxygenic photosynthesis) and the production of atmospheric O_2 in turn leading to the suppression of MIF sulfur isotopes. However, increases in chemical weathering and primary productivity may have drawn down atmospheric CO_2 (Berner and Maasch, 1996) and atmospheric CH_4 from atmospheric oxidative reactions (Pavlov et al., 2003). A general reduction of greenhouse effects could have triggered the first glaciation event of the Paleoproterozoic.

Several diamictites in the lowest parts of the Paleoproterozoic Snowy Pass and Huronian Supergroups (Canada) record a widespread glacial event. Figure 15 shows a compilation of $\Delta^{33}S$, $\delta^{34}S_{sulfide}$ and $\delta^{13}C_{carb}$ data from Paleoproterozoic sedimentary rocks and their relation to the estimated timing of these diamictites. Recognizing that compilations of isotopic data are subject to sample biases, geographical effects and age uncertainties, they nevertheless provide crucial information bearing on (albeit gross) changes in environmental conditions. The estimated timing of the glaciations is based on previously proposed correlations between North American and South African glacial diamictites and more geochronological data are forthcoming to support these correlations (Bekker et al., 2004; Dorlan, 2004; Hannah et al., 2004). The Ramsey Lake diamictite is stratigraphically the lowest recognized glacial tillite in the Huronian Supergroup, which is constrained by the 2.45 Ga U-Pb age of the underlying Copper Cliff rhyolite (Krogh et al., 1984) and by the Nipissing diabase sills and dykes with an age of 2.22 Ga and which intrudes the entire sequence (Corfu and Andrews, 1986). Diamictites of the Campbell Lake Formation (the lowest of three tillites in the Snowy Pass Supergroup) have been correlated with the Ramsey Lake diamictite (Young, 1973; Roscoe and Card, 1993). These diamictites have not been correlated with other Paleoproterozoic diamictites and may indicate that this glaciation event was extensive, but not global. During the glaciation event, passive volcanic emission of CO_2 would have gradually increased greenhouse effects in the atmosphere and led to thawing (Kirschvink et al., 2000;

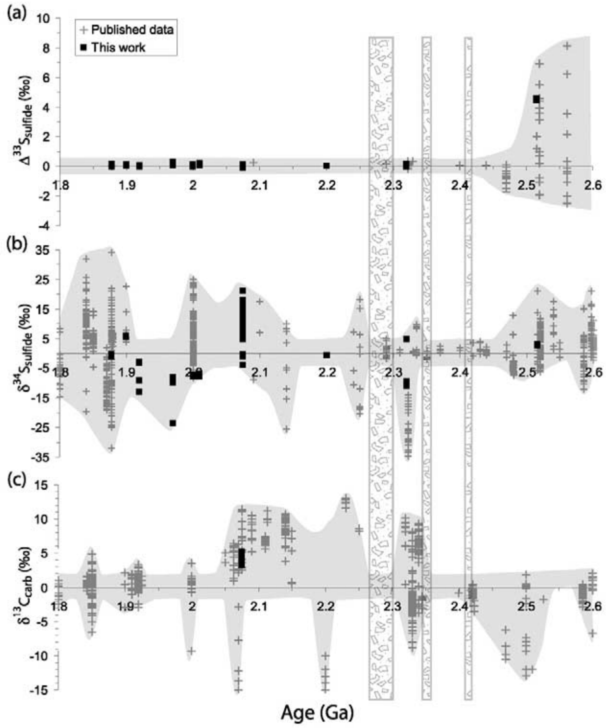

Fig. 15. Biogeochemical coevolution of Paleoproterozoic sulfur and carbon isotopes (from sulfides and carbonates, respectively) and their relation to approximate timing of glaciations. Gray crosses = published data; black boxes = our new data. (a) Compilation of published and new $\Delta^{33}S$ data for sulfides from Paleoproterozoic sedimentary rocks. (b) Compilation of published and new $\delta^{34}S$ data for sulfides from Paleoproterozoic sediments (modified from Canfield and Raiswell, 1999). (c) Published and new $\delta^{13}C$ data from Paleoproterozoic carbonates (excludes carbonates with poor age constraints). Each interpretive envelope is drawn assuming default range of values for $\Delta^{33}S_{sulfide}$ (−0.30 to +0.30‰), $\delta^{34}S_{sulfide}$ (−5 to +5‰), and $\delta^{13}C_{carb}$ (−3 to +3‰) for periods where no data are available. Ages plotted are averages of known age constraints for each data point; error bars omitted for simplicity.

Hoffman and Schrag, 2002). Consequently, increased erosion rates and nutrient delivery to the oceans would have stimulated increased primary productivity and another period of atmospheric O_2 accumulation. Therefore we propose that such events in the aftermath of Paleoproterozoic glaciations have strongly influenced atmospheric levels of O_2, CH_4 and CO_2 with the following effects (Fig. 15 and summarized in Fig. 16):

(1) a decrease in the abundance of atmospheric CH_4 from oxidation with O_2 and photolytically-produced OH and O radicals (Pavlov et al., 2003);

(2) a decrease in atmospheric concentration of CO_2 due to enhanced biologic carbon fixation and chemical weathering of silicates;

(3) the demise of MIF sulfur isotopes in sulfides (Bekker et al., 2004).

We propose that widespread carbon fixation by oxygenic photosynthesis along with the oxidation of atmospheric CH_4 after the first glaciation could have contributed to trigger the second glaciation of the Paleoproterozoic.

Diamictites from the Bruce Formation, second tillite in the Huronian Supergroup, and from the Vagner Formation, second in the Snowy Pass Supergroup, have been chronostratigraphically correlated (Young, 1973; Roscoe and Card, 1993). A diamictite above the unconformity at the base of the 2.43–2.32 Ga Duitschland Formation in the Transvaal Supergroup may be tentatively correlated with the second glaciation (Bekker et al., 2001; Hannah et al., 2004). The $\delta^{13}C_{carb}$ in the Duitschland Formation varies from −3 to +10‰, which is consistent with enhanced primary productivity after the glacial event (Buick et al., 1998; Bekker et al., 2001). Because there are relatively few correlative glacial diamictites of that age, it is possible that the second Paleoproterozoic glaciation was extensive but not necessarily global. Subsequently, passive atmospheric CO_2 accumulation from volcanism created a greenhouse that terminated the second glaciation. Similar to the aftermath of the first glaciation, increased erosion rates augmented nutrient delivery to the ocean and stimulated oxygenic photosynthesis to produce O_2. It appears that atmospheric O_2 levels after the second glacial event were sufficiently high to inhibit MIF of sulfur isotopes as observed in sedimentary pyrite nodules from the Timeball Hill Formation in the Transvaal Supergroup (Bekker et al., 2004). Pyrite nodules from the lower parts of the Timeball Hill Formation have a Re-Os age of 2.32 Ga (Hannah et al., 2004). Yet, various avenues existed through which atmospheric O_2 could have decreased between the second and third glaciations. Increased weathering combined with oxidation of crustal sulfides during thawing of the second Paleoproterozoic glaciation increased sulfate delivery to the ocean. It is well established that the concentration of dissolved sulfate tempers the magnitude of sulfur isotopic fractionation by microbial sulfate reduction (MSR). Recent studies have shown that MSR imparts minimal sulfur isotopic fractionation when sulfate concentrations are below 200 μM (Habicht et al., 2002). Typically, when sulfate concentration is nonlimiting, MSR can lead to $\delta^{34}S$ values between −4 to −46‰ for hydrogen sulfide (Canfield and Raiswell, 1999). Isotopically light $\delta^{34}S$ values down to −35‰ measured in sulfides from the 2.32 Ga Timeball Hill Fm (Fig. 15b) point to MSR under nonlimiting sulfate concentrations (Cameron, 1982; Bekker et al., 2004). Figure 15b shows that the record of sulfur isotopes in sulfides during the

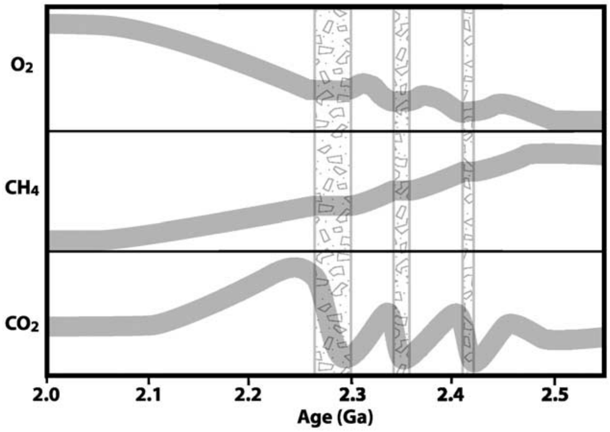

Fig. 16. Proposed model for fluctuations in concentration of O_2, CH_4, and CO_2 in Paleoproterozoic atmosphere plotted with respect to estimated timing of glaciations.

Paleoproterozoic is woefully inadequate and emphasizes the need for more data from other sedimentary rocks to trace the evolution of $\delta^{34}S_{sulfide}$ and by inference, fluctuations in seawater sulfate concentration and/or in $\delta^{34}S_{sulfate}$ at this time. We propose in our schematic in Figure 16 that atmospheric CO_2 and CH_4 levels once more decreased after the second glacial event in response to the photosynthetic production of O_2, which may have triggered a third glaciation.

The last documented Paleoproterozoic glaciation is well represented by the diamictite of the Gowganda Formation (Huronian Supergroup), which is older than 2.22 Ga (Corfu and Andrews, 1986). Other diamictites can be correlated with the Gowganda Formation and include the Fern Creek, Enchantment Lake and Reany Creek diamictites of the Marquette Supergroup (Ojakangas, 1983, 1988) and the Headquarters diamictite of the Snowy Pass Supergroup (Young, 1973; Roscoe and Card, 1993). The Chibougamau diamictite (Chibougamau area, Québec) has been tentatively correlated with the Gowganda Formation (Long, 1981). Glacially derived sediments of the upper part of the Timeball Hill and Boshoek Fms. in the Transvaal Basin are correlated with the Makganyene diamictite in the Griqualand West Basin (Bekker et al., 2001; Hannah et al., 2004). The Makganyene Fm conformably underlies the volcanic rocks of the Ongeluk Formation, which has been directly correlated to the Hekpoort volcanics that overlie the Boshoek Formation. The Hekpoort volcanics have zircon populations of different ages, but one group of concordant zircon U-Pb data indicate an age of 2.25 Ga (Dorlan, 2004). Correlation between the Ongeluk Formation and the Hekpoort Formation could indicate that the Makganyene diamictite was syn-depositional with the Timeball Hill diamictite and that these diamictites are related to the North American diamictites of the third Paleoproterozoic glaciation. Paleomagnetic studies indicate a near-equatorial paleolatitude for the Ongeluk andesite and hence for the near-contemporaneous Makganyene diamictite (Evans et al., 1997). Negative $\delta^{13}C_{carb}$ values were measured in the marine sediments of the Hotazel Formation ($\delta^{13}C_{carb}$ from −15 to −5‰), which overlies the Makganyene diamictite. These results are consistent with the oxidation of organic matter accumulated in the anoxic oceans of the Snowball Earth (Kirschvink et al., 2000). Unfortunately, because of the poor age constraints for other Paleoproterozoic diamictites, it is not possible to specifically correlate a glaciation event with the Lammos diamictite (Pechenga Group; Negrutsa and Negrutsa, 1981), the Padlei diamictite (Hurwitz Group; Young and McLennan, 1981), the Black Hills diamictite (Rapid City area, South Dakota; Kurtz, 1981), the Meteorite Bore diamictite (Mount Bruce Supergroup; Martin, 1999) or the Urkkavaara diamictite (Karelian Supergroup; Marmo and Ojakangas, 1984). We propose that the third glaciation was the penultimate global cooling event in the Paleoproterozoic and required massive amounts of atmospheric CO_2 for its eventual termination (Pierrehumbert, 2004).

4.4. Atmospheric Oxygen after the Paleoproterozoic Glaciations

Melting of the third and largest of the Paleoproterozoic glaciations would have led to increased erosion rates and delivery of nutrients to the oceans, thereby stimulating oxygenic photosynthetic blooms to produce massive quantities of atmospheric O_2. Atmospheric CO_2 and CH_4 levels went down due to carbon fixation, chemical weathering and oxidation (Fig. 16). Two sulfide grains from the 2.22–2.43 Ga Sompujärvi quartzite schist FI02055 were found to have $\delta^{34}S$ values indicative of sedimentary sulfur and near-zero $\Delta^{33}S$ values, consistent with the presence of O_2 above 10^{-5} PAL level in the atmosphere at that time. We acknowledge that the relatively poor age constraints for the Sompujärvi Formation cannot be used to prove a relation with the third glaciation (as shown in Figure 15a). Results for the Gamohaan and Sompujärvi Fms. definitively show that the loss of MIF sulfur isotopes occurred between 2.52 and 2.22 Ga and during the periods of glaciation. Carbonates precipitated in the aftermath of the third glacial event remained ^{13}C-enriched for ~200 Ma from ~2.25 to 2.05 Ga (Fig. 15c; Karhu and Holland, 1996). Evidence for this global-scale Paleoproterozoic $\delta^{13}C_{carb}$ excursion has been found on many continents and is particularly well represented in Baltica where isotopically heavy carbonates are found in several sequences including the Peräpohja and Kuusamo schist belts (Karhu, 1993), the Tulomozerskaya Formation near Lake Onega (Melezhik et al., 1999), and the Pechenga and Imandra-Varzuga belts of the Kola Peninsula (Karhu and Melezhik, 1992). Examples in the Peräpohja belt include dolomite from the 2.16–2.30 Ga Misi schist belt with $\delta^{13}C$ values of up to +13‰, dolomite from the ~2.09 Ga Kvartsimaa Formation with $\delta^{13}C$ around +9‰ and the 2.06–2.09 Ga Rantamaa dolomite with $\delta^{13}C$ values up to +11‰ (Karhu, 1993; Fig. 7).

Figure 15b shows that during the global $\delta^{13}C_{carb}$ excursion $\delta^{34}S$ values down to −25‰ are found in the Silverton Formation of the Transvaal Supergroup (Cameron, 1982) and in the Lorrain and Gordon Lake Fms. of the Huronian Supergroup (Hattori et al., 1983, 1985). Very negative $\delta^{34}S$ data in sedimentary sulfides probably mean elevated seawater sulfate concentrations after the glaciations and suggest that oxidative weathering of crustal sulfides was an important sink for O_2. Samples from the Rantamaa Formation analyzed in this work were found to have a range of $\delta^{34}S$ values larger than ~25‰, pointing to a sedimentary origin for the sulfur. Such a large range of positive $\delta^{34}S$ values probably track fluctuations in the concentration of seawater sulfate and/or $\delta^{34}S_{sulfate}$. The near-zero $\Delta^{33}S$ values of these sulfides are related to an atmosphere with O_2 concentrations above the 1 ppm level of Pavlov and Kasting (2002). Our results for the oxygen and carbon isotopic compositions suggest that metamorphism is not likely to have significantly affected the sulfur isotopic composition of the sulfides. The $\delta^{18}O$ values range over ~4‰, which may be due to interactions with warm fluids (Valley, 1986) during the metamorphic history of the Rantamaa Formation. The small range of $\delta^{13}C_{carb}$ values observed (+3.28 to +5.25‰) is consistent with previously reported carbon isotopes for this formation (Karhu, 1993) and indicates that the carbon isotopic composition likely remained constant during metamorphic recrystallization and decarbonation reactions. The apparent lack of covariation between $\delta^{18}O_{carb}$ and $\delta^{13}C_{carb}$ suggest that postdepositional processes may have modified the oxygen isotopes of the carbonate, but that the carbon isotopes record a period of enhanced carbon burial and primary productivity at time of sedimentation. Sulfur isotopes indicate that atmospheric O_2 levels remained sufficiently elevated to suppress MIF despite possible variations in rates of oxidation of crustal sulfides. Metamorphism affected the morphologies of sulfides studied from the Rantamaa Formation, but probably did not significantly modify their δ^{34}S values. There may exist a covariation between $\delta^{13}C_{carb}$ and $\delta^{34}S_{sulfide}$ but, as seen in Figure 11, more data would be needed to confirm this.

Our δ^{34}S values around −8‰ of sulfides from the black shales FIK64-2 and FIK19-A are consistent with a sedimentary origin and we would argue therefore that their Δ^{33}S values (all close to 0‰) indicate relatively high atmospheric O_2 concentrations inhibiting MIF of sulfur isotopes at time of deposition. Isotopically light δ^{34}S values measured in the quartz rock FIK118-2 and black shale FIK119-8 specify relatively high seawater sulfate concentration and therefore the near-zero Δ^{33}S data likewise suggest high atmospheric O_2 concentrations during sedimentation. Similarly, δ^{34}S values of sulfides analyzed in FIK97-7 and FIK97-11 are in line with a sedimentary origin and near-zero Δ^{33}S values point to abundant O_2 in the atmosphere. New data plotted in Figure 15a show that Δ^{33}S data in postglaciation sediments do not record MIF sulfur isotopes. Atmospheric O_2 levels remained higher than 10^{-5} PAL even in the face of significant oxidative weathering. Our Δ^{33}S data for sulfides from Finland, combined with the other correlative measures cited above, constitute strong evidence for an irreversible increase of O_2 in the atmosphere after the Paleoproterozoic glaciations.

5. CONCLUSIONS

We report 152 analyses of multiple sulfur isotopes on seven sulfide standards and performed 83 analyses on 69 individual sulfide grains from 30 different Paleoproterozoic samples. Combined use of high spatial resolution techniques such as electron microprobe and secondary ion mass spectrometry in multicollection mode enables for high sample throughput and the ability to select specific sulfide target areas for isotopic analyses while uniquely preserving petrographic context. Our results provide independent confirmation of the loss of MIF sulfur isotope in sediments between 2.52 and 2.22 Ga (Farquhar et al., 2000; Mojzsis et al., 2003; Bekker et al., 2004). We propose a model for the Paleoproterozoic that integrates published $\delta^{13}C_{carb}$, $\delta^{34}S_{sulfide}$ and Δ^{33}S data and information on the estimated timing of glaciations. We propose that the beginning of the oxygenation of the atmosphere was triggered by the break-up of a Late Archean supercontinent, which led to increased erosion rates and nutrient delivery to the oceans. These conditions are suspected to have stimulated blooms of oxygenic photosynthesis, led to massive organic carbon generation and burial, a drop in CO_2 and the rise of atmospheric O_2. Increases of free O_2 were probably detrimental to atmospheric CH_4 abundances and we propose that this could have been responsible for starting a series of glaciation cycles. On the basis of possibly correlative stratigraphic sequences from North America and South Africa, we estimate the timing of these glaciations and propose that global cooling was in part governed by blooms of oxygenic photosynthesis and fluctuations in the levels of greenhouse gases. The concentration of O_2 in the atmosphere was likely altered by the oxidation of CH_4 in the atmosphere and oxidation of other reduced species in the crust and hydrosphere. We further suggest that the population expansion of aerobic eukaryotes and other organisms requiring O_2 for respiration (e.g., sulfide oxidizers, nitrifyers and methanotrophs) played an important role in regulating O_2. Following the cycle of glaciations, a global $\delta^{13}C_{carb}$ excursion between 2.05 and 2.25 Ga resulted in a significant increase of atmospheric O_2 (Karhu and Holland, 1996). The end of the $\delta^{13}C_{carb}$ excursion is well-represented by the Rantamaa Formation in northern Finland. We found a δ^{34}S range of ~25‰ in sulfides from the Rantamaa rocks, which indicates a sedimentary source of sulfur. Combined with near-zero Δ^{33}S values, this indicates that atmospheric O_2 concentrations remained above Archean values after the period of Paleoproterozoic glaciations. It is interesting to note that this period of time represents the first documented appearance of large eukaryotic forms (Han and Runnegar, 1992; Shixing and Huineng, 1995), which probably flourished in response to the increased levels of atmospheric O_2. If our hypothesis is correct, the cycle of glaciations and episodic periods of atmospheric O_2 accumulation in the Paleoproterozoic was terminated at least in part by the culmination of a biogeochemical balance between CO_2-fixing-O_2-producing oxygenic photosynthesizers and O_2-breathing-CO_2-emitting organisms. Other aerobic metabolisms requiring O_2 as a terminal electron acceptor such as sulfide oxidation, nitrification and methanotrophy would have been favored by these global environmental redox changes. These redox variations can be traced using the geochemistry of Fe isotopes in shales, banded iron formations and perhaps Fe-rich dolomites occurring in Paleoproterozoic sedimentary successions (Rouxel et al., 2005). Molybdenum isotopes could be used to trace biogeochemical redox changes in the Paleoproterozoic environment, in a way similar to studies of Mesoproterozoic sediments (Anbar and Knoll, 2004; Arnold et al., 2004). This discussion highlights the importance of performing more stable isotopic analyses on Paleoproterozoic sediments from geographically distant regions. Future work will be needed to test the possible global nature of some Paleoproterozoic glaciations, to trace the high-resolution evolution of Δ^{33}S within glacial intervals, to measure $\delta^{34}S_{sulfide}$ as a proxy for fluctuations in seawater sulfate concentrations and/or in $\delta^{34}S_{sulfate}$ and to relate these measures to a separate redox proxy such as the nitrogen cycle. The transition from an anoxic world in the Archean to the oxygenated environments of the Proterozoic and beyond prompted the rise of aerobic microorganisms and ultimately led to the emergence of the complex multicellular life.

Acknowledgments—We thank M. Grove, G. Jarzebinski and A. Schmitt for technical assistance with the ion microprobe and D. Trail for help with analyses. J. Drexler and P. Boni are thanked for their assistance with the electron microprobe and sample preparation, respectively. We are grateful to J. W. Schopf (UCLA) for kindly providing sample PPRG1414 and to P. K. Strother (Boston College) for donating sample GF7. D. E. Canfield generously provided us with his δ^{34}S database. We thank N. Kortelainen for her preliminary carbon and oxygen isotopic data of the Rantamaa Formation. This manuscript benefited from discussions with A. A. Pavlov. Constructive reviews from J. L. Kirschvink and two anonymous reviewers and editorial handling by L. R. Kump greatly improved this manuscript. This work is supported by a cooperative agreement between the NASA Astrobiology Institute (NAI) and the University of Colorado Center for Astrobiology (SJM). The UCLA ion microprobe facility is supported by a grant from the National Science Foundation Instrumentation and Facilities Program. KM acknowledges support from the UCLA Center for Astrobiology. DP acknowledges graduate support from the NAI and the Fonds de recherche sur la nature et les technologies du Québec.

Associate editor: L. R. Kump

REFERENCES

Altermann W. and Nelson D. R. (1998) Sedimentation rates, basin analysis and regional correlations of three Neoarchaean and Paleoproterozoic sub-basins of the Kaapvaal craton as inferred from precise U-Pb zircon ages from volcaniclastic sediments. *Sed. Geol.* **120,** 225–256.

Anbar A. D. and Knoll A. H. (2004) Proterozoic ocean chemistry and evolution: A bioinorganic bridge? *Science* **297,** 1137–1142.

Arnold G. L., Anbar A. D., Barling J., and Lyons T. W. (2004) Molybdenum isotope evidence for widespread anoxia in Mid-Proterozoic oceans. *Science* **304,** 87–90.

Barghoorn E. S. and Tyler S. A. (1965) Microorganisms from the Gunflint Chert. *Science* **147,** 563–577.

Beaumont V. and Robert F. (1999) Nitrogen isotope ratios of kerogens in Precambrian cherts: A record of the evolution of atmosphere chemistry? *Precamb. Res.* **96,** 63–82.

Bekker A., Kaufman A. J., Karhu J. A., Beukes N. J., Swart Q. D., Coetzee L. L., and Eriksson K. A. (2001) Chemostratigraphy of the Paleoproterozoic Duitschland Formation, South Africa: Implications for coupled climate change and carbon cycling. *Am. J. Sci.* **301,** 261–285.

Bekker A., Karhu J. A., Eriksson K. A., and Kaufman A. J. (2003a) Chemostratigraphy of Paleoproterozoic carbonate successions of the Wyoming Craton: Tectonic forcing of biogeochemical change? *Precamb. Res.* **120,** 279–325.

Bekker A., Sial A. N., Karhu J. A., Ferreira V. P., Noce C. M., Kaufman A. J., Romano A. W., and Pimentel M. M. (2003b) Chemostratrigraphy of carbonates from the Minas Supergroup, Quadrilátero Ferrífero (iron quadrangle), Brazil: A stratigraphic record of Early Proterozoic atmospheric, biogeochemical and climatic change. *Am. J. Sci.* **303,** 865–904.

Bekker A., Holland H. D., Wang P.-L., Rumble D. III, Stein H. J., Hannah J. L., Coetzee L. L., and Beukes N. J. (2004) Dating the rise of atmospheric oxygen. *Nature* **427,** 117–120.

Bekker A., Kaufman A. J., Karhu J. A., and Eriksson K. A. (2005) Evidence for Paleoproterozoic cap carbonates in North America. *Precamb. Res.* **137,** 167–206.

Berner R. A. and Maasch K. A. (1996) Chem. weathering and controls on atmospheric O_2 and CO_2: Fundamental principles were enunciated by J. J. Ebelmen in 1845. *Geochim. Cosmochim. Acta* **60,** 1633–1637.

Brocks J. J., Logan G. A., Buick R., and Summons R. E. (1999) Archean molecular fossils and the early rise of eukaryotes. *Science* **285,** 1033–1036.

Buick I. S., Uken R., Gibson R. L., and Wallmach T. (1998) High-$\delta^{13}C$ Paleoproterozoic carbonates from the Transvaal Supergroup, South Africa. *Geology* **26,** 875–878.

Cameron E. M. (1982) Sulphate and sulphate reduction in early Precambrian oceans. *Nature* **296,** 145–148.

Cameron E. M. and Garrels R. M. (1980) Geochemical compositions of some Precambrian shales from the Canadian shield. *Chem. Geol.* **28,** 181–197.

Canfield D. E. and Raiswell R. (1999) The evolution of the sulfur cycle. *Am. J. Sci.* **299,** 697–723.

Canfield D. E., Habicht K. S., and Thamdrup B. (2000) The Archean sulfur cycle and the early history of atmospheric oxygen. *Science* **288,** 658–661.

Chamberlain K. R. (1998) Medicine Bow orogeny: Timing of deformation and model of crustal structure produced during continent-arc collision, ca. 1.78 Ga, southeastern Wyoming. *Rocky Mountain Geol.* **33,** 259–277.

Chaussidon M. (1988) Géochimie du soufre dans le manteau et la croûte océanique: Apports de l'analyse isotopique in situ par sonde ionique. Ph.D. dissertation. Centre de recherches pétrographiques et géochimiques, CNRS.

Chaussidon M. and Lorand J. P. (1990) Sulphur isotope composition of orogenic spinel lherzolite massifs from Ariege (North-Eastern Pyrenees, France): An ion microprobe study. *Geochim. Cosmochim. Acta* **54,** 2835–2846.

Claesson S., Huhma H., Kinny P. D., and Williams I. S. (1993) Svecofennian detrital zircon ages—Implications for the Precambrian evolution of the Baltic Shield. *Precamb. Res.* **64,** 109–130.

Corfu F. and Andrews A. J. (1986) A U-Pb age for mineralized Nipissing diabase, Gowganda, Ontario. *Can. J. Earth Sci.* **23,** 107–109.

Crowe D. E. and Vaughan R. G. (1996) Characterization and use of isotopically homogenous standards for in situ laser microprobe analysis of $^{34}S/^{32}S$ ratios. *Am. Mineral.* **81,** 187–193.

DesMarais D. J., Strauss H., Summons R. E., and Hayes J. M. (1992) Carbon isotope evidence for the stepwise oxidation of the Proterozoic environment. *Nature* **359,** 605–609.

Ding T., Valkiers S., Kipphardt H., De Bièvre P., Taylor P. D. P., Gonfiantini R., and Krouse R. (2001) Calibrated sulfur isotope abundance ratios of three IAEA sulfur isotope reference materials and V-CDT with a reassessment of the atomic weight of sulfur. *Geochim. Cosmochim. Acta* **65,** 2433–2437.

Dorlan H. (2004) Provenace, age and timing of sedimentation of selected Neoarchean and Paleoproterozoic successions on the Kaapvaal Craton. Ph.D. thesis. Rand Afrikaans University.

Evans D. A., Beukes N. J., and Kirschvink J. L. (1997) Low-latitude glaciation in the Palaeoproterozoic era. *Nature* **386,** 262–266.

Farquhar J., Bao H., and Thiemens M. H. (2000) Atmospheric influence of Earth's earliest sulfur cycle. *Science* **289,** 756–758.

Farquhar J., Savarino J., Airieau S., and Thiemens M. H. (2001) Observation of wavelength-sensitive mass-independent sulfur isotope effects during SO_2 photolysis: Implications for the early atmosphere. *J. Geophys. Res.* **106,** 32829–32839.

Farquhar J., Wing B. A., McKeegan K. D., Harris J. W., Cartigny P., and Thiemens M. H. (2002) Mass-independent sulfur of inclusions in diamond and sulfur recycling on Earth Earth. *Science* **298,** 2369–2372.

Farquhar J., Johnston D. T., Wing B. A., Habicht K. S., Canfield D. E., Airieau S., and Thiemens M. H. (2003) Multiple sulfur isotopic interpretations of biosynthetic pathways: Implications for biological signatures in the sulfur isotope record. *Geobiology* **1,** 27–36.

Farquhar J. and Wing B. A. (2003) Multiple sulfur isotopes and the evolution of the atmosphere. *Earth Planet. Sci. Lett.* **213,** 1–13.

Fralick P., Davis D. W., and Kissin S. A. (2002) The age of the Gunflint Formation, Ontario, Canada: Single zircon U-Pb age determinations from reworked volcanic ash. *Can. J. Earth Sci.* **39,** 1085–1091.

Greenwood J. P., Mojzsis S. J., and Coath C. D. (2000) Sulfur isotopic composition of individual sulfides in Martian meteorites ALH84001 and Nakhla: Implications for crust-regolith exchange on Mars. *Earth Planet. Sci. Lett.* **184,** 23–35.

Habicht K. S., Gade M., Thamdrup B., Berg P., and Canfield D. E. (2002) Calibration of sulfate levels in the Archean ocean. *Science* **298,** 2372–2374.

Han T. M. and Runnegar B. (1992) Megascopic eukaryotic algae from the 2.1-billion-year-old Negaunee iron-formation, Michigan. *Science* **257,** 232–235.

Hannah J. L., Bekker A., Stein H. J., Markey R. J., and Holland H. D. (2004) Primitve Os and 2316 Ma age for marine shale: Implications of Paleoproterozoic glacial events and the rise of atmospheric oxygen. *Earth Planet. Sci. Lett.* **225,** 43–52.

Hattori K., Krouse H. R., and Campbell F. A. (1983) The start of sulfur oxidation in continental environments: About 2.2×10^9 years ago. *Science* **221,** 549–551.

Hattori K., Campbell F. A., and Krouse H. R. (1985) Sulphur isotope abundances in sedimentary rocks, relevance to the evolution of the Precambrian atmosphere. *Geokhimiya* **6,** 834–849.

Heaman L. M. (1997) Global magmatism at 2.45 Ga: Remnants of an ancient large igneous province? *Geology* **25,** 299–302.

Hoffman P. F. and Schrag D. P. (2002) The snowball Earth hypothesis: Testing the limits of global change. *Terra Nova* **14,** 129–155.

Holland H. D. (1984) *The Chemical Evolution of the Atmosphere and Oceans.* Princeton University Press, Princeton.

Hu G., Rumble D. III, and Wang P. L. (2003) An ultraviolet laser microprobe for the in situ analysis of multisulfur isotopes and its use in measuring Archean sulfur isotope mass-independent anomalies. *Geochim. Cosmochim. Acta* **67,** 3101–3117.

Huhma H., Cliff R. A., Perttunen V., and Sakko M. (1990) Sm-Nd and Pb isotopic study of mafic rocks associated with early Proterozoic continental rifting: The Peräpohja schist belt in northern Finland. *Contrib. Mineral. Petrol.* **104,** 369–379.

Huhma H. (1986) Sm-Nd, U-Pb and Pb-Pb isotopic evidence for the origin of the Early Proterozoic Svecokarelian crust in Finland. *Geol. Surv. Finland Bull.* **337,** 48pp.

Hulston J. R. and Thode H. G. (1965) Variations in the ^{33}S, ^{34}S and ^{36}S contents of meteorites and their relation to chemical and nuclear effects. *J. Geophys. Res.* **70,** 3475–3484.

Karhu J. A. (1993) Paleoproterozoic evolution of the carbon isotope ratios of sedimentary carbonates in the Fennoscandian Shield. *Geol. Surv. Finland Bull.* **371,** 87 pp.

Karhu J. A. (2005) Paleoproterozoic carbon isotope excursion. In *Precambrian Geology of Finland—Key to the Evolution of the Fennoscandian Shield* (eds. M. Lehtinen, P. A. Nurmi and O. T. Rämö), pp. 669–680. Elsevier, Amsterdam.

Karhu J. A. and Melezhik V. A. (1992) Carbon isotope systematics of early Proterozoic sedimentary carbonates in the Kola Peninsula, Russia: Correlations with Jatulian formations in Karelia. In *Correlation of Precambrian Formation of the Kola-Karelia Region and Finland* (eds. V. V. Balagansky and F. P. Mitrofanov), pp. 48–53. Kola Scientific Centre of the Russian Academy of Sciences, Apatity.

Karhu J. A. and Holland H. D. (1996) Carbon isotopes and the rise of atmospheric oxygen. *Geology* **24,** 867–870.

Kirschvink J. L., Gaidos E. J., Bertani L. E., Beukes N. J., Gutzmer J., Maepa L. N., and Steinberger R. E. (2000) Paleoproterozoic snowball Earth: Extreme climatic and geochemical global change and its biological consequences. *Proc. Natl. Acad. Sci. U S A* **97,** 1400–1405.

Koistinen T. J. (1981) Structural evolution of an early Proterozoic stata-bound Cu-Co-Zn deposit, Outokumpu, Finland. *Trans. R. Soc. Edinburgh Earth Sci.* **72,** 115–158.

Kortelainen N. (1998) Peräpohjan liuskealueen paleoproterotsooisten sedimenttisten karbonaattikivien kerrostumisympäristön luonne, hiilen isotooppikoostumus ja hivenalkuainekemia (in Finnish). M.Sc. thesis. University of Helsinki.

Krogh T. E., Davis D. W., and Corfu F. (1984) Precise U-Pb zircon and baddeleyite ages for the Sudbury area. In *The Geology and Ore Deposits of the Sudbury Structure* (eds. E. G. Pye, A. J. Naldrett and P. E. Gilblin), pp. 431–446. Special Paper 1. Ontario Geological Survey.

Kurtz D. D. (1981) Early Proterozoic diamictites of the Black Hills, South Dakota. In *Earth's Pre-Pleistocene Glacial Record* (eds. M. J. Hambrey and W. B. Harland), pp. 800–802. Cambridge University Press, Cambridge.

Lindsay J. F. and Brasier M. D. (2002) Did global tectonics drive early biosphere evolution? Carbon isotope record from 2.6 to 1.9 Ga carbonates of Western Australian basins. *Precamb. Res.* **114,** 1–34.

Long D. G. F. (1981) Glaciogenic rocks in the Early Proterozoic Chibougamau Formation of northern Québec. In *Earth's Pre-Pleistocene Glacial Record* (eds. M. J. Hambrey and W. B. Harland), pp. 817–820. Cambridge University Press, Cambridge.

Loukola-Ruskeeniemi K. (1991) Geochemical evidence for the hydrothermal origin of sulphur, base metals and gold in Proterozoic metamorphosed black shales, Kainuu and Outokumpu areas, Finland. *Min. Dep.* **26,** 152–164.

Loukola-Ruskeeniemi K., and Heino T. (1996) Geochemistry and genesis of the black shale-hosted Ni-Cu-Zn deposit at Talvivaara, Finland. *Econ. Geol.* **91,** 80–110.

Lukkarinen H. and Lundqvist T. (2000) Karelian domain. In *Description to the Bedrock Map of Central Fennoscandia (Mid-Norden)* (eds. T. Lundqvist and S. Autio), pp. 26–47. Special Paper 28. Geological Survey of Finland.

Mäkelä M. (1974) A study of sulfur isotopes in the Outokumpu ore deposit, Finland. *Geol. Surv. Finland Bull.* **267,** 45pp.

Marmo J. S. and Ojakangas R. W. (1984) Lower Proterozoic glaciogenic deposits, eastern Finland. *Geol. Soc. Am. Bull.* **95,** 1055–1062.

Martin D. M. (1999) Depositional setting and implications of Paleoproterozoic glaciomarine sedimentation in the Hamersley Province, Western Australia. *Geol. Soc. Am. Bull.* **111,** 189–203.

Melezhik V. A., Fallick A. E., and Clark T. (1997) Two billion year old isotopically heavy carbon: Evidence from the Labrador Trough, Canada. *Can. J. Earth. Sci.* **34,** 271–285.

Melezhik V. A., Fallick A. E., Medvedev P. V., and Makarikhin V. V. (1999) Extreme $^{13}C_{carb}$ enrichment in ca. 2.0 Ga magnesite-stromatolite-dolomite-"red beds" association in a global context: A case for the world-wide signal enhanced by a local environment. *Earth Sci. Rev.* **48,** 71–120.

Mojzsis S. J., Coath C. D., Greenwood J. P., McKeegan K. D., and Harrison T. M. (2003) Mass-independent isotope effects in Archean (2.5 to 3.8 Ga) sedimentary sulfides determined by ion microprobe analysis. *Geochim. Cosmochim. Acta* **67,** 1635–1658.

Negrutsa T. F. and Negrutsa V. Z. (1981) Early Proterozoic Lammos tilloids of the Kola Peninsula, USSR. In *Earth's Pre-Pleistocene Glacial Record* (eds. M. J. Hambrey and W. B. Harland), pp. 678–670. Cambridge University Press, Cambridge.

Ohmoto H. (1986) Stable isotope geochemistry of ore deposits. In *Stable Isotopes in High Temperature Geological Processes* (eds. J. W. Valley, H. P. Taylor and J. R. O'Neil), pp. 491–559. Reviews in Mineralogy 16. Mineralogical Society of America, Washington, D.C.

Ohmoto H. and Goldhaber M. B. (1997) Sulfur and carbon isotopes. In *Geochemistry of Hydrothermal Ore Deposits* (ed. H. L. Barnes), pp. 517–611. Wiley, New York.

Ojakangas R. W. (1983) Evidence for Early Proterozoic glaciation: The dropstone unit—Diamictite association. In *Proterozoic Exogenic Processes and Related Metallogeny* (eds. K. Laajoki and J. Paakkola), pp. 53–72. Bulletin 331. Geological Survey of Finland.

Ojakangas R. W. (1988) Glaciation: An uncommon "mega-event" as a key to intracontinental and intercontinental correlation of Early Proterozoic basin fill, North American and Baltic cratons. In *New Perspectives in Basin Analysis* (eds. K. L. Kleinspehn and C. Paola), pp. 431–444. Springer-Verlag, New York.

Ono S., Eigenbrode J. L., Pavlov A. A., Kharecha P., Rumble D. III, Kasting J. F., and Freeman K. H. (2003) New insights into Archean sulfur cycle from mass-independent sulfur isotope records from the Hamersley Basin, Australia. *Earth Planet. Sci. Lett.* **213,** 15–30.

Papineau D., Mojzsis S. J., Karhu J. A., and Marty B. (2005) Nitrogen isotopic composition of ammoniated phyllosilicates: Case studies from Precambrian metamorphosed sedimentary rocks. *Chem. Geol.* **216,** 37–58.

Pavlov A. A. and Kasting J. F. (2002) Mass-independent fractionation of sulfur isotopes in Archean sediments: Strong evidence for an anoxic Archean atmosphere. *Astrobiology* **2,** 27–41.

Pavlov A. A., Hurtgen M. T., Kasting J. F., and Arthur M. A. (2003) Methane-rich Proterozoic atmosphere? *Geology* **31,** 87–90.

Perttunen V. and Vaasjoki M. (2001) U-Pb geochronology of the Peräpohja Schist Belt, northwestern Finland. In *Radiometric Age Determinations from Finnish Lapland and Their Bearing on the Timing of Precambrian Volcano-Sedimentary Sequences* (ed. M. Vaasjoki), pp. 45–84. Special Paper 33. Geological Survey of Finland.

Pierrehumbert R. T. (2004) High levels of atmospheric carbon dioxide necessary for the termination of global glaciation. *Nature* **429,** 646–649.

Rastas P., Huhma H., Hanski E., Lehtonen M. I., Härkönen I., Kortelainen V., Mänttäri I., and Paakkola J. (2001) U-Pb isotopic studies on the Kittilä greenstone area, central Lapland, Finland. In *Radiometric Age Determinations from Finnish Lapland and Their Bearing on the Timing of Precambrian Volcano-Sedimentary Sequences* (ed. M. Vaasjoki), pp. 95–141. Special Paper 33. Geological Survey of Finland.

Roscoe S. M. and Card K. D. (1993) The reappearence of the Huronian in Wyoming: Rifting and drifting of ancient continents. *Can. J. Earth Sci.* **30,** 2475–2480.

Rouxel O. J., Bekker A., and Edwards K. J. (2005) Iron isotope constraints on the Archean and Paleoproterozoic ocean redox state. *Nature* **307,** 1088–1091.

Russell W. A., Papanastassiou D. A., and Tombrello T. A. (1978) Ca isotope fractionation on the Earth and other solar system materials. *Geochim. Cosmochim. Acta* **42,** 1075–1090.

Shixing Z. and Huineng C. (1995) Megascopic multicellular organisms from the 1700-million-year-old Tuanshanzi Formation in the Jixian area, North China. *Science* **270,** 620–622.

Sreenivas B., Das Sharma S., Kumar B., Patil D. J., Roy A. B., and Srinivasan R. (2001) Positive δ^{13}C excursion in carbonate and organic fractions from the Paleoproterozoic Aravalli Supergroup, Northwestern India. *Precamb. Res.* **106,** 277–290.

Strauss H. and Moore T. B. (1992) Abundances and isotopic compositions of carbon and sulfur species in whole rock and kerogen samples. In *The Proterozoic Biosphere: A Multidisciplinary Study* (eds. J. W. Schopf and C. Klein), pp. 709–798. Cambridge University Press, Cambridge.

Valley J. W. (1986) Stable isotope geochemistry of metamorphic rocks. In *Stable Isotopes in High Temperature Geological Processes* (eds. J. W. Valley, H. P. Taylor and J. R. O'Neil), pp. 445–489. Reviews in Mineralogy 16. Mineralogical Society of America, Washington, D.C.

Young G. M. (1973) Tillites and aluminous quartzites as possible time markers for middle Precambrian (Aphebian) rocks of North America, pp. 97–127. Special Paper 12. Geological Association of Canada.

Young G. M. and McLennan S. M. (1981) Early Proterozoic Padlei Formation, Northwest Territories, Canada. In *Earth's Pre-Pleistocene Glacial Record* (eds. M. J. Hambrey and W. B. Harland), pp. 790–794. Cambridge University Press, Cambridge.

Young E. D., Galy A., and Nagahara H. (2002) Kinetic and equilibrium mass-dependent isotope fractionation laws in nature and their geochemical and cosmochemical significance. *Geochim. Cosmochim. Acta* **66,** 1095–1104.

Zhao G., Cawood P. A., Wilde S. A., and Sun M. (2002) Review of global 2.1–1.8 Ga orogens: Implications for a pre-Rodinia supercontinent. *Earth-Sci. Rev.* **59,** 125–162.